AN EXTERNAL DOSE RECONSTRUCTION INVOLVING A RADIOLOGICAL DISPERSAL DEVICE

A Dissertation

by

DAVID WAYNE HEARNSBERGER

Submitted to the Office of Graduate Studies of
Texas A&M University
in partial fulfillment of the requirements for the degree of

DOCTOR OF PHILOSOPHY

December 2006

Major Subject: Nuclear Engineering

AN EXTERNAL DOSE RECONSTRUCTION INVOLVING A RADIOLOGICAL DISPERSAL DEVICE

A Dissertation

by

DAVID WAYNE HEARNSBERGER

Submitted to the Office of Graduate Studies of
Texas A&M University
in partial fulfillment of the requirements for the degree of

DOCTOR OF PHILOSOPHY

Approved by:

Co-Chairs of Committee,	Ian S. Hamilton
	John Poston, Sr.
Committee Members,	Les Braby
	Mike Walker
	Rita Moyes
Head of Department,	William Burchill

December 2006

Major Subject: Nuclear Engineering

ABSTRACT

An External Dose Reconstruction Involving a Radiological Dispersal Device.

(December 2006)

David Wayne Hearnsberger, B.S., Texas A&M University;

M.S., Texas A&M University

Co-Chairs of Advisory Committee: Dr. Ian S. Hamilton
Dr. John W. Poston, Sr.

Recent events have underscored the need for the United States government to provide streamlined emergency response procedures and subsequent dose estimations for personnel responding to incidents involving radioactive material. Indeed, the National Council on Radiation Protection and Measurements Report No. 138 (NCRP 2001) indicates that exposures received by first responders will be important for a number of reasons, including planning for the appropriate use of key personnel in an extended emergency situation. In response, the Department of Homeland Security has published Protective Action Guides (DHS 2006) to help minimize these exposures and associated risks.

This research attempts to provide some additional radiological exposure knowledge so that an Incident Commander, with limited or no information, can make more informed decisions about evacuation, sheltering-in-place, relocation of the public, turn-back levels, defining radiation hazard boundaries, and in-field radiological dose assessments of the radiation workers, responders, and members of the public. A method to provide such insight begins with providing a model that describes the physics of radiation interactions, radiation source and geometry, collection of field measurements, and interpretation of the collected data. A Monte Carlo simulation of the model is performed so that calculated

results can be compared to measured values.

The results of this investigation indicate that measured organ absorbed doses inside a tissue equivalent phantom compared favorably to the derived organ absorbed doses measured by the Panasonic thermoluminescence dosimeters and with Monte Carlo 'N' Particle modeled results. Additionally, a Victoreen 450P pressurized ion chamber measured the integrated dose and these results compared well with the Panasonic right lateral TLD. This comparison indicates that the Victoreen 450P ionization chamber could potentially serve as an estimator of real-time effective dose and organ absorbed dose, if energy and angular dependence corrections could be taken into account. Finally, the data obtained in this investigation indicate that the MCNP model provided a reasonable method to determine organ absorbed dose and effective dose of a simulated Radiological Dispersal Device in an Inferior-Superior geometry with $Na^{99m}TcO_4$ as the source of radioactive material.

ACKNOWLEDGMENTS

For me, the completion of this dissertation represents the level of perseverance that God asks all of us to display for Him. More than ever, I realize that God, our Creator, possesses all things, events, and knowledge. Without God's divine wisdom and His son, Jesus Christ's loving sacrifice, I could never hope to have been able to endure the time and effort required to complete this work and bring it to finality. For His love, I am extremely grateful.

While completing this work, God also saw fit to bless me with a wonderful wife and family. My beautiful wife, Christina, and four extraordinary children, Austin, Aaron, Ashley, and Adam have all sacrificed parts of their lives to help me complete this work. I wish to recognize their special love and sacrifice because it most certainly is made of God's love. Without God and my family, I have nothing and am nothing. With God and my family in my life, I am blessed more richly than anyone.

I do not want to diminish the vast amount of support of others involved in this work, however. Dr. John Poston and Dr. Ian Hamilton have supported me throughout my entire eleven year-long college-level academic career. In some regards I am sure they are ready to see me leave and continue onward, but had it not been for God using them as a vessel to constantly encourage and support me, I fear that I would not have been able to finish this research. Dr. Rita Moyes who also served on my Master of Science Committee provided many long hours of consultation and support.

There are so many people for whom I am thankful for helping complete this chapter in my life and I know my time and space are limited to describe my thanks. Vanasa McCallister (Modisette) has inspired me beyond belief by showing me what perseverance means by enduring years of personal hardship. Her sister, Wendy Sorrells (Modisette)

helped me find God in my life again and for that my life is saved. Their parents, Dee and Elaine Modisette certainly are responsible for being my “adopted” parents over the last sixteen years. They will all hold a part of my heart and I wish everyone could be as fortunate as I am to have people like this in my life. Rachael Huntley (Clifton) has inspired me to keep working even when times are their most difficult. She attended undergraduate school with me, left after graduation to attend the American Academy of Dramatic Arts in New York, NY and Los Angeles, Ca., endured some personal tragedy, and still continued to work towards her dream. She can be seen in the movie, entitled “Mr. and Mrs. Smith.” Finally, there is Veronica McCaffrey who currently works for the Department of State and is working overseas on assignment. She continues to sacrifice for the freedom the citizens of our country take for granted on a daily basis. For her, I hope that this work will lead to further advancements to help continue keeping our citizens safe from those who wish to do us harm.

Finally, several organizations require recognition as well. The US Air Force has graciously donated its time and facilites to provide the dosimeters and dosimeter reading systems needed to collect the data analyzed in this research. Both Dade Moeller and Associates and Earth Tech have donated facilities and funding that allowed me to work away from home on nights, weekends, and in some cases, different states. God’s hand is in all things and I am grateful that He provided a way to help these organizations meet the demands placed by this research.

TABLE OF CONTENTS

Page

ABSTRACT iii

ACKNOWLEDGMENTS v

TABLE OF CONTENTS vii

LIST OF FIGURES x

LIST OF TABLES xii

I. INTRODUCTION 1

II. BACKGROUND 5

II.1 Gamma Ray Physics and Radiation Sources 5

II.2 Sodium Pertechnetate Background Information 7

II.3 Principles of Thermoluminescence Dosimetry 8

II.3.a Phosphors 8

II.3.b General Characteristics of Dosimeters 10

II.3.b (1) Precision and Bias 10

II.3.b (2) Dose Range 10

II.3.b (3) Dose-Rate Range 11

II.3.b (4) Stability 11

II.3.b (5) Energy Dependence 12

II.3.b (6) Angular Dependence 14

II.3.c Randall-Wilkins Theory 18

II.3.d Trap Stability 20

II.3.e Intrinsic Efficiency of TLD Phosphors 20

II.4 MCNP Simulation 20

Page

II.4.a Tally Cards 21
II.4.b MCNP Geometry Definitions 22
II.4.c Materials Description Cards 22
II.4.d Source Definition Card 22
II.4.e Variance Reduction Techniques 23
II.4.f The Dispersal Model 24
II.4.g The Phantom Model 26
III. MATERIALS AND METHODS 28
III.1 Preparation of the Source Geometry 28
III.2 Preparation of the Rando® Phantom 28
III.3 Basis for the Selection of Sodium Pertechnetate 32
III.4 Basis for the Selection of Oleic Acid 33
III.5 Delivery of the $Na^{99m}TcO_4$ 33
III.6 Full Circle MCNP Simulation 35
IV. RESULTS 36
IV.1 DXT-RAD Dosimeter Results 36
IV.2 Panasonic UD-802A TLD Results 40
IV.3 Full Circle Modeling Results 46
IV.4 Radiological Monitoring Results 50
V. DISCUSSION 52
V.1 Comparison of Energy and Angular Corrected Values Versus Non-Corrected Values 52
V.2 Model Validation 53

Page

V.3 Verification of ICRP Conversion Coefficients……..53

V.3.a Description of Panasonic TLD-Derived Organ-Absorbed Dose Results 53

V.3.b Comparison of DXT-RAD Results to Panasonic TLD Results 55

V.4 Discussion of Full Circle Organ-Absorbed Dose Results..... 56

V.5 Comparison of Panasonic TLD Results to Victoreen 450P Values 57

V.6 Significance to First Responders 58

V.7 Importance to the Incident Commander..... 59

VI. CONCLUSIONS..... 61

REFERENCES 64

APPENDIX A 67

APPENDIX B 77

APPENDIX C 79

VITA..... 93

LIST OF FIGURES

Page

Figure 1: Logic flow used to validate the MCNP model, verify ICRP Report No. 74 conversion coefficients, and determine the organ absorbed doses. 4

Figure 2: The ^{99m}Tc decay scheme from the Nuclear Data Sheets. 6

Figure 3: Probability of interaction of photons with a given energy versus the effective atomic number (After Attix 1986). 7

Figure 4: Energy-level diagram of the thermoluminescence process (after Attix 1986). 9

Figure 5: Typical energy-dependence curves in terms of the response per unit exposure of x- or γ-rays (taken after Attix 1986). 13

Figure 6: Thermoluminescent response of LiF per roentgen and per rad for photon energies from 6 to 2800 keV (after Attix 1986). 14

Figure 7: Definition of the angle, α, subtended by incident radiation (after ICRP 1996). 15

Figure 8: The angular variation of effective dose for photons; effective dose per unit air kerma in free air, E/K_a, for monoenergetic parallel photon beams incident at various angles on an adult anthropomorphic computational model (ICRP 1996). 17

Figure 9: A thermoluminescence glow curve versus temperature (after Attix 1986). . 19

Figure 10: Inferior-superior ^{99m}Tc exposure geometry for the Rando® phantom. 24

Figure 11: MCNP model depicting layered water, olive oil, and $Na^{99m}TcO_4$ and room barriers. 25

Figure 12: MCNP modeled adult male human body. 27

Figure 13: Photograph of the Rando® phantom. 29

Figure 14: Monitoring period number one, organ-specific absorbed dose results. 39

Figure 15: Monitoring period number two, organ-specific absorbed dose results. 40

Page

Figure 16: Graphical representation of the data from Table 7 45

Figure 17: Graphical representation of the data from Table 8 45

Figure 18: Graphical representation of the data fromTable 9 49

LIST OF TABLES

Page

Table 1: Phantom numbering convention for TLD placement per slice. 30

Table 2: Panasonic UD-802 TLD package description. 31

Table 3: Organ absorbed dose for monitoring periods 1 and 2, uncorrected for energy and angular dependence. 37

Table 4: Organ absorbed dose for monitoring periods 1 and 2, corrected for energy and angular dependence. 38

Table 5: Panasonic UD-802 TLD results. 41

Table 6: Organ absorbed doses derived from Panasonic UD-802 TLDs compared to DXT-RAD dosimeters. 43

Table 7: Organ absorbed doses derived from Panasonic UD-802 TLDs compared to DXT-RAD dosimeters. 44

Table 8: MCNP results for the full disk simulation. 48

Table 9: Victoreen 450P dose rate and integrated dose measurements for monitoring period number one. 50

Table 10: Victoreen 450P dose rate and integrated dose measurements for monitoring period number two. 51

Table A1: Monitoring period one DXT-RAD results. 67

Table A2: Monitoring period two DXT-RAD results. 72

Table B1: Radiological monitoring parameters for monitoring period one. 77

Table B1: Radiological monitoring parameters for monitoring period two. 78

Table C1: The measured and calculated absorbed dose results for the small intestine 79

Table C2: The measured and calculated absorbed dose results for the kidney 80

Table C3: The measured and calculated absorbed dose results for the liver 81

Page

Table C4: The measured and calculated absorbed dose results for the ascending colon 82

Table C5: The measured and calculated absorbed dose results for the transverse colon 82

Table C6: The measured and calculated absorbed dose results for the gall bladder ... 83

Table C7: The measured and calculated absorbed dose results for the pancreas 83

Table C8: The measured and calculated absorbed dose results for the right lung 84

Table C9: The measured and calculated absorbed dose results for the small intestine 86

Table C10: The measured and calculated absorbed dose results for the kidney..... 87

Table C11: The measured and calculated absorbed dose results for the liver 88

Table C12: The measured and calculated absorbed dose results for the ascending colon 89

Table C13: The measured and calculated absorbed dose results for the transverse colon 89

Table C14: The measured and calculated absorbed dose results for the gall bladder . 90

Table C15: The measured and calculated absorbed dose results for the pancreas 90

Table C16: The measured and calculated absorbed dose results for the right lung 91

I. INTRODUCTION

With increased awareness of terrorist activities that seek to compromise the United States domestically, and our interests abroad, the need to provide streamlined emergency response procedures and subsequent dose estimates for personnel responding to incidents involving radioactive material has never been more important. In response to this growing awareness, several United States (US) government agencies have set out to develop procedures and plans for incidents involving radiological dispersal devices (RDD) and/or improvised nuclear devices (IND). For instance, the Environmental Protection Agency (EPA) is developing a Radiation Playbook that provides guidance for On-Scene Coordinators (OSC) on how to collect radiological data during the initial few hours after the onset of a radiological incident. The Department of Energy (DOE) has published, through the Federal Radiological Monitoring and Assessment Center (FRMAC), three assessment manuals, two monitoring manuals, an emergency operations manual, and a health and safety manual. Other agencies have published information but, in all cases, the plans and procedures must be developed according to the National Response Plan (NRP) managed by the Department of Homeland Security (DHS) (NRP December 2004) .

With documents such as the NRP, the National Contingency Plan (NCP) and the National Incident Management System (NIMS), there is literally a sea of information available to anyone interested in federal radiological emergency response. The “person in charge” of responding to incidents requiring federal involvement is known as the Incident Commander (IC). In a scenario involving RDDs or INDs, the IC (after a time) is a member of the FBI (FBI, 1998) during the period of crisis management. If such a device is

---

This dissertation follows the style and format of Health Physics.

detonated, then the consequence management period begins and the IC changes to state and local authorities and federal authorities such as the EPA OSC or a representative from the Federal Emergency Management Agency (FEMA). The IC relies on local, county, state, and federal agencies for information needed to determine whether to recommend ad hoc respiratory protection, evacuation, relocation, or shelter-in-place for those who may become collaterally involved in such an incident. For example, Musolino and Harper (2006) provided modeling and measurement information derived from the data collected from over 500 explosive experiments involving about twenty different materials with eighty-five device geometries to develop recommendations for the early phase response. They recommend the evacuation of the public occur at a 50-year committed dose of 500 mSv (50 rem), while DHS (2006) and EPA (1992) recommend evacuation occur at 50 mSv (5 rem), but should begin at 10 mSv (1 rem). Another example is that Musolino and Harper (2006) recommend sheltering in place at a 50-year committed dose of 50 mSv (5 rem) and the DHS and EPA recommend sheltering at 10 mSv to 50 mSv (1 rem to 5 rem) but should normally begin at 10 mSv (1 rem). It is interesting to note that in terms of life-saving efforts and/or protection of critical infrastructure, EPA (1992) recommends a maximum dose equivalent of 250 mSv (25 rem) while NCRP (2001), with proper risk information provided, recommends a maximum dose equivalent of 500 mSv (50 rem).

Note, however, that collection and interpretation of radiological data are two of the most important factors when designing radiological emergency plans, and procedures. The most important information needed by the IC are the magnitude and extent of the projected dose. Whether the information provided is expressed in terms of dose rate, radioactive airborne concentration, loose surface contamination levels, or values derived from direct-reading radiation detection instrumentation for external penetrating radiation, the

information that guides an IC to a decision is the projected dose. Musolino and Harper (2006) state that strategies and decisions to protect emergency responders, based on projected dose and dose rate, must be made in the planning stages rather than just after an attack occurs.

The objectives of this research are:

- simulate a planar source of radioactivity similar to that produced by a radiological dispersal device;
- measure the external radiation exposure at selected locations on the surface of a suitable phantom;
- measure the organ doses inside a suitable phantom due to this radiation field;
- relate the above results with measurements made with a portable ionization chamber (x-ray and gamma-ray radiation); and
- compare the measured results with those obtained through Monte Carlo simulation of the exposure geometry.

The Monte Carlo code can be used to model the source of radiation, assumed geometry, radiation transport, internal organs of the body, and to calculate the absorbed dose to selected internal organs. The organ absorbed doses are calculated using the Monte Carlo N-Particle, Version 4C (Briesmeister 2000). The experiment measured the organ absorbed dose and also estimated the effective dose at four different locations on the outside of a tissue-equivalent phantom.

Figure 1 shows the logic flow used to validate the MCNP model, verify International Commission on Radiological Protection (ICRP) Report No. 74 (ICRP 1996) conversion coefficients, and how organ absorbed dose was determined. Verification of ICRP Report No. 74 conversion coefficients involved comparing the derived organ absorbed dose obtained using Panasonic UD-802 TLDs to the MCNP-calculated organ absorbed dose.

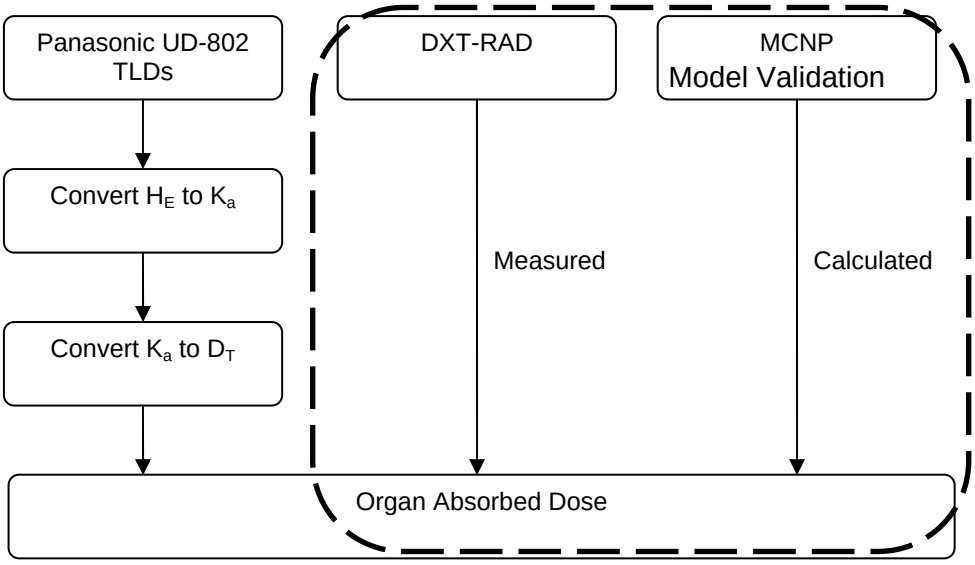

Figure 1: Logic flow used to validate the MCNP model, verify ICRP Report No. 74 conversion coefficients, and determine the organ absorbed doses**.**

The dashed lined area in Figure 1 represents the process used to validate the MCNP results. The DXT-RAD dosimeters measured organ absorbed dose inside the Rando® phantom and MCNP code coupled with the anthropomorphic phantom provided calculated organ absorbed doses.

The left-side of Figure 1 shows the process used to predict the effective dose on the outside of the body and thus the organ absorbed dose. ICRP (1996) provides conversion coefficients to convert effective dose to free-in-air kerma, and free-in-air kerma to absorbed dose. The converted organ absorbed dose can be compared to measured and MCNP-calculated values to determine the accuracy with which an externally mounted dosimeter can be used to predict organ absorbed dose.

II. BACKGROUND

II.1 Gamma Ray Physics and Radiation Sources

The radiation source chosen for this investigation was technetium. All isotopes of technetium are man-made and all are radioactive (Nuclides and Isotopes 2002). The specific isotope of technetium used in this experiment was the metastable form of technetium-99 (^{99m}Tc) in the chemical form of sodium pertechnetate ($Na^{99m}TcO_4$). The primary gamma-ray energy of the ^{99m}Tc is approximately 140 keV with an absolute yield of 89.06 percent. Figure 2 shows the relative abundance of this gamma ray is 100 percent, and the authors of the Nuclear Data Sheets indicate that to determine the absolute abundance, one should multiply the relative abundance by a factor of 0.8906 (Tuli *et al,* 2001).

Although gamma rays of this energy predominantly interact with air, water, and tissue via the Compton Scattering effect, photoelectric interactions occur as well. Identification of these events is important because they describe the interaction processes the gamma rays undergo to deposit energy in the body. Deposition of this energy results in absorbed dose. Figure 3 shows the interaction regions for the gamma ray energies from 0.01 MeV to 100 MeV.

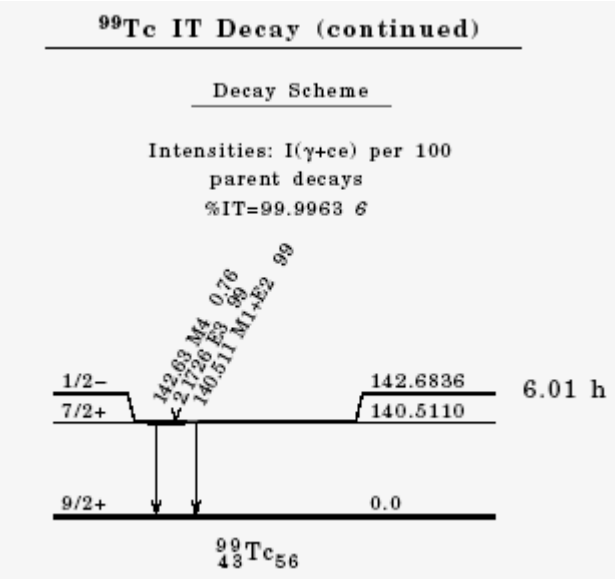

Figure 2: The ^{99m}Tc decay scheme from the Nuclear Data Sheets.

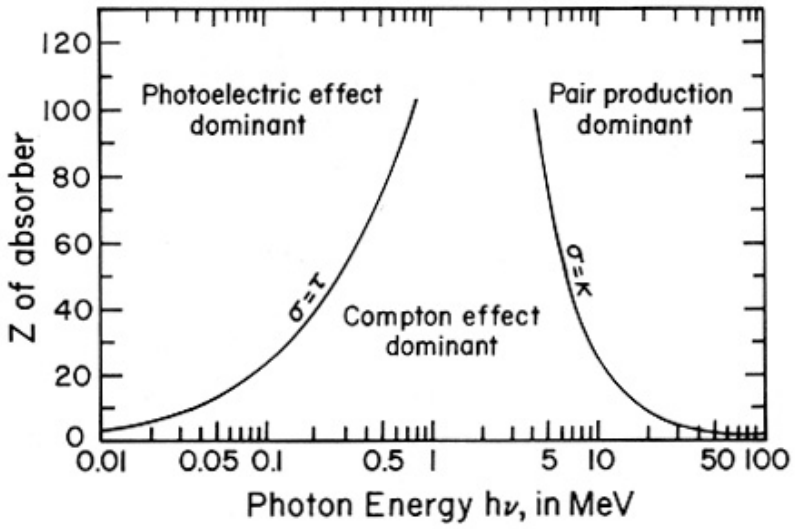

Figure 3: Probability of interaction of photons with a given energy versus the effective atomic number (After Attix 1986).

II.2 Sodium Pertechnetate Background Information

The $Na^{99m}TcO_4$ used in this study is a very common radiopharmaceutical and is the most widely used radiodiagnostic agent in use today (Shikata and Iguchi, 1986). Typically, the ^{99m}Tc is chemically separated from the parent radionuclide, molybdenum-99 (^{99}Mo), inside a portable chromatographic generator by adsorbing the ^{99}Mo on an alumina column and rinsing the less strongly bound, water soluble TcO^-_4 ion at key intervals with isotonic saline (Monroy-Guzman *et al* 2003). The total activity may vary from generator to generator depending upon the needs of the recipient, but one may assume that about 740 GBq (about 20 Ci) of ^{99m}Tc in the form of $Na^{99m}TcO_4$ can be obtained from a typical

generator* .

II.3 Principles of Thermoluminescence Dosimetry

Considered by many to be a separate branch of science, radiation dosimetry literally means, radiation dose measurement. The goal of radiation dosimetry is to establish the energy deposited per unit mass in a suitable receptor. Quantitative measurements involve using various types of dosimeters and evaluation systems to retrieve the information stored in the dosimetry system. Experiments conducted for this study used thermoluminescence dosimeters (TLD). As the name implies, heat is used to evaluate ("read") the thermoluminescence dosimeters to retrieve the stored information in the TLD. More specifically, the TLDs used were lithium fluoride crystals doped with magnesium and titanium impurities (LiF:Mg,Ti, also called TLD-100).

II.3.a Phosphors

TLDs are made of small crystalline dielectric insulator material that contains interstitial defects in the crystal structure. These interstitial defects give the dielectric its thermoluminescence properties. For TLD-100, the interstitial defects are caused by the introduction of magnesium (Mg) and titanium (Ti) into the crystal – expressed as LiF:(Mg, Ti). These interstitial defects serve two purposes.

Interstitial defects in the crystal structure create "traps" and "holes." The traps retain electrons while the holes can capture and hold the charge carriers in a potential energy well for long periods of time. The other purpose of the defects is to create luminescence centers, located at either electron traps or the hole traps, which emit light when the electrons or holes are permitted to recombine. Attix (1986) provides a convenient

* Personal communication with Danny Allen of NuTech, 2003

energy-level diagram to understand this phenomenon in Figure 4 below.

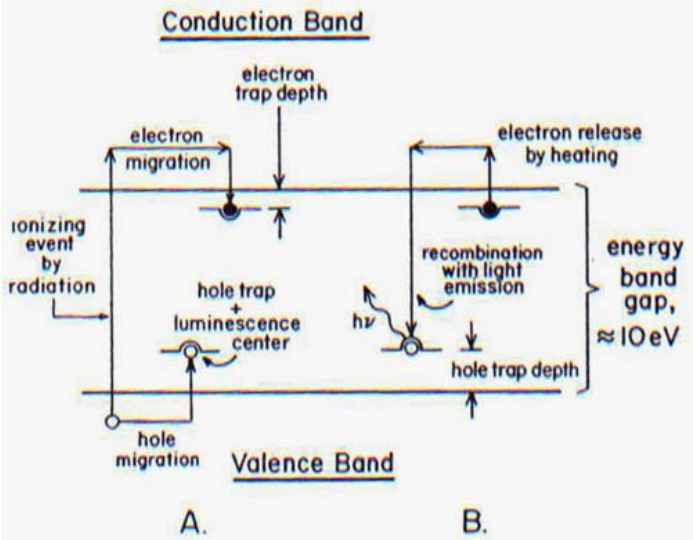

Figure 4: Energy-level diagram of the thermoluminescence process (after Attix 1986).

Part A in Figure 4 depicts phosphor excitation by radiation (i.e., raising an electron into the conduction band, where it migrates to an electron trap). The hole that is left behind migrates to a hole trap. During the heating process to "read" the TLD (depicted in Part B), assuming the electron is at a more shallow trapping depth than the hole, the electron is released first into the conduction band and migrates into a hole trap. The hole trap may be assumed to act as a luminescence center, or closely coupled to one, such that the recombining of the electron with the luminescence center releases a visible light photon (Attix 1986). One may further assume that the intensity of the released visible light photons

is directly proportional to the amount of radiant energy deposited.

II.3.b General Characteristics of Dosimeters

There are several general characteristics of dosimeters, but the discussion will be limited to the characteristics relevant for this investigation.

II.3.b (1) Precision and Bias

In the context of radiation dosimetry, precision is better defined to mean reproducibility. The precision of a radiation dosimeter concerns random fluctuations in instrument characteristics, ambient conditions, the stochastic nature of a radiation field, etc. For clarity, a high precision implies a low standard deviation (Attix 1986). Whereas the precision describes how closely a single measurement compares to the expected value, accuracy expresses how closely the expected value compares to the true value. To state that a dosimeter is a precise measuring instrument is to mean that it is capable of very good measurement reproducibility if deployed correctly. To state that a dosimeter is a very accurate instrument is to mean that freedom from error is relatively high (i.e., the dosimeter is relatively unbiased).

II.3.b (2) Dose Range

To be useful, a dosimeter must have an ability to detect doses over the range of interest. The dosimeter should exhibit a well-established relationship between the actual and indicated doses. For many dosimeters, this is a linear relationship. Ideally, this property should be expressed from doses as low as about ten μGy (1 mrad) to about 1000 Gy (about 100,000 rad). The upper limit is generally a physical limitation of the particular dosimeter. For example, some of the physical limitations are the following (Attix 1986):

- Exhaustion of the supply of atoms, molecules, or solid-state entities ("traps") being acted upon by the radiation producing the reading;
- Competing reactions by radiation products, for example in chemical dosimeters; and
- Radiation damage to the dosimeter (e.g., discoloration of light-emitting dosimeters, or damage to electrical insulators).

Mostly, the upper limit of the dose range is manifested by a deviation from the well-established dosimeter response.

II.3.b (3) Dose-Rate Range

The absorbed dose is the parameter of interest in this research. Since the radiation exposure continued throughout an extended period, an integrating-type dosimeter is necessary to measure the absorbed dose. It is also necessary that the dosimeter response should be independent of dose rate. Since the activity used in this experiment produces moderate levels of dose, one need not be concerned with a low-dose rate limitation such as that presented by insulator leakage current in an ion chamber or such limitations in a photographic film dosimeter. Moreover, the high dose rate limitations caused by charged particle tracks being created closely enough together in space and time (volumetric recombination) to allow the electron-hole pairs to interact between tracks is not a significant concern for this experiment for the same reason.

II.3.b (4) Stability

The foregoing characteristics of a dosimeter should be stable both before and after irradiation. With regard to "prior-to-use" irradiation periods, the dosimeter should retain its sensitivity when exposed to variable ambient changes in temperature, atmospheric pressure, humidity, and light (Pederson *et al* 1995). The TLD-100 material used in this experiment exhibits a gradual sensitivity change due to migration and rearrangement of the

trapping centers in the phosphor, but this is controlled by the annealing process. In contrast, the TLD-100 can experience a “fading” effect after irradiation, and before it is read, by losing some of the trapped charge carriers. Normally, to correct for this fading, all the TLDs are “read” at the same time after irradiation. The annealing process adds additional energy to eliminate the very low-energy traps, making the TLD more stable and reducing the fading.

II.3.b (5) Energy Dependence

Generally speaking, one would desire that the dosimeter used does not have a response that is dependent upon the incident radiation energy being measured. This is often not the case, however. For photons with an energy significantly below 100 keV and for a dosimeter that has an effective atomic number greater than that of air, one finds that the dosimeters have a tendency to over-respond as shown in Figure 5.

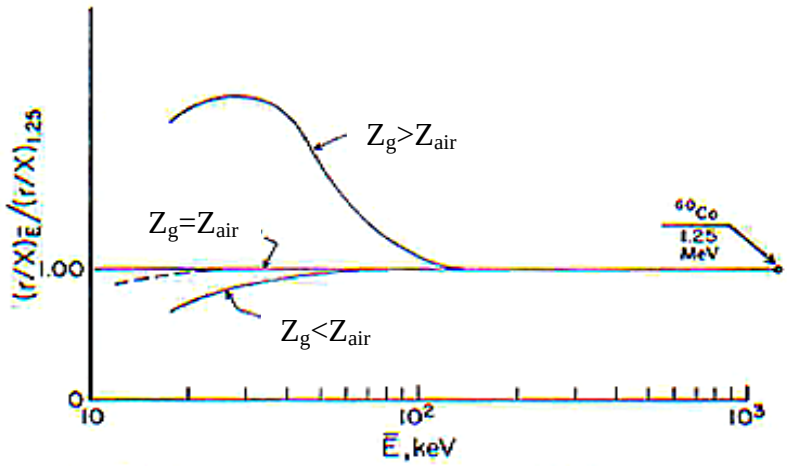

Figure 5: Typical energy-dependence curves in terms of the response per unit exposure of x- or γ-rays (taken after Attix 1986).

In the experiment conducted with $Na^{99m}TcO_4$, the 140-keV photon has an energy dependent response of about 1.0 in air, relative to cobalt-60 gamma rays. The rise in response below 100 keV is due to the domination of photoelectric interactions. The small decreases at the left end of the graph are due to photoelectric effect and attenuation in the dosimeter. Figure 6 shows the actual (instead of typical) energy-dependent response of the TLD-100 material. Figure 6 indicates that the thermoluminescence (TL) response per rad is about 1.08, or about eight percent over-response due to 140 keV photons. An over-response factor of 1.08 is assumed in these experiments, since the exact energy of the impinging gamma rays on the TLDs is not known.

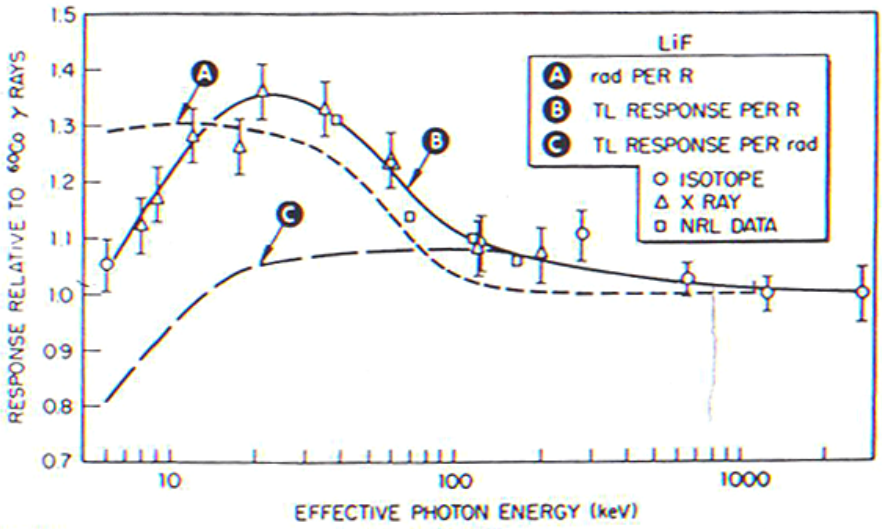

Figure 6: Thermoluminescent response of LiF per roentgen and per rad for photon energies from 6 to 2800 keV (after Attix 1986).

II.3.b (6) Angular Dependence

One of three operational dose quantities defined by the International Commission on Radiation Units and Measurements (ICRU) (ICRU 1985, 1988, 1992, 1993), directional dose equivalent (H'(d, α)), is related to the ICRP Report No. 60 protection quantities (ICRP 1991). In general, operational quantities are related to protection quantities by measurement and calculation using radiation weighting factors, tissue weighting factors, and anthropomorphic phantoms (ICRP 1996). In this instance, directional dose equivalent is an operational quantity, whose response to the angle of the incident radiation will affect the results of the protection quantity, organ absorbed dose. In this investigation, the over-response or under-response of a dosimeter was taken into account by applying organ – and geometry – specific conversion coefficients developed in ICRP Report No. 74 (ICRP

1996). Figure 7 below shows the subtended angle, α, that the incident radiation makes with an individual dosimeter. Understanding this phenomenon is important since the subtended angle of the incident radiation can result in a lower than expected deposition of energy, which will result in an underestimation of the absorbed dose.

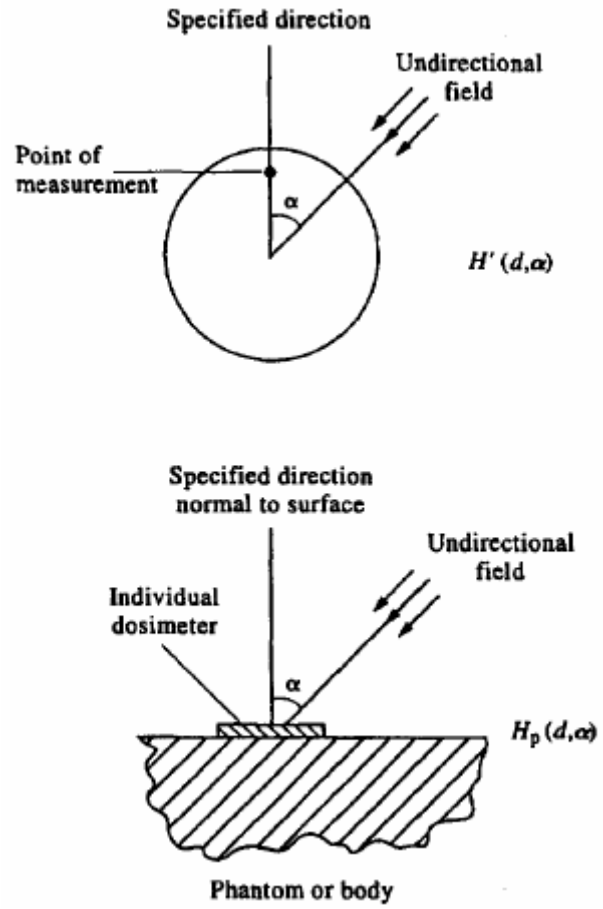

Figure 7: Definition of the angle, α, subtended by incident radiation (after ICRP 1996).

ICRP (1996) discusses five fundamental exposure geometries, i.e., anterior-posterior (AP), posterior-anterior (PA), lateral (LAT for left and right), rotational (ROT), and isotropic (ISO). In the rotational (ROT) geometry, a unidirectional radiation field is applied while the slab or anthropomorphic phantom is rotated in either a clockwise or a counter-clockwise direction. As the phantom rotates about the vertical axis, the angle of incident radiation changes from zero to 360 degrees. ICRP (1996) states in paragraph 144 that:

> the ROT geometry is seen as an approximation to irradiation from a widely dispersed planar source (e.g. as would be likely from environmental contamination).

While not all dosimeter measurements can be conducted at all angles of incidence during this rotational process, one can approximate the changes in dosimeter response based on a few pre-selected locations on the phantom.

The proposed Inferior-Superior (IS) geometry provides a surrogate to the ROT geometry for applying correction factors to dosimeters exposed at varying angles to photon radiation. In this case, the incident angle of radiation from the ground surface to the dosimeter changes from zero degrees to a maximum of sixty-three degrees since the radius of the radioactive source is three meters and the point of dosimetric interest on the phantom is approximately 1.5 meters in height. Figure 8, from ICRP (1996), shows the angular response for varying photon energies. The direction of incidence is orthogonal to the transverse axis of the body.

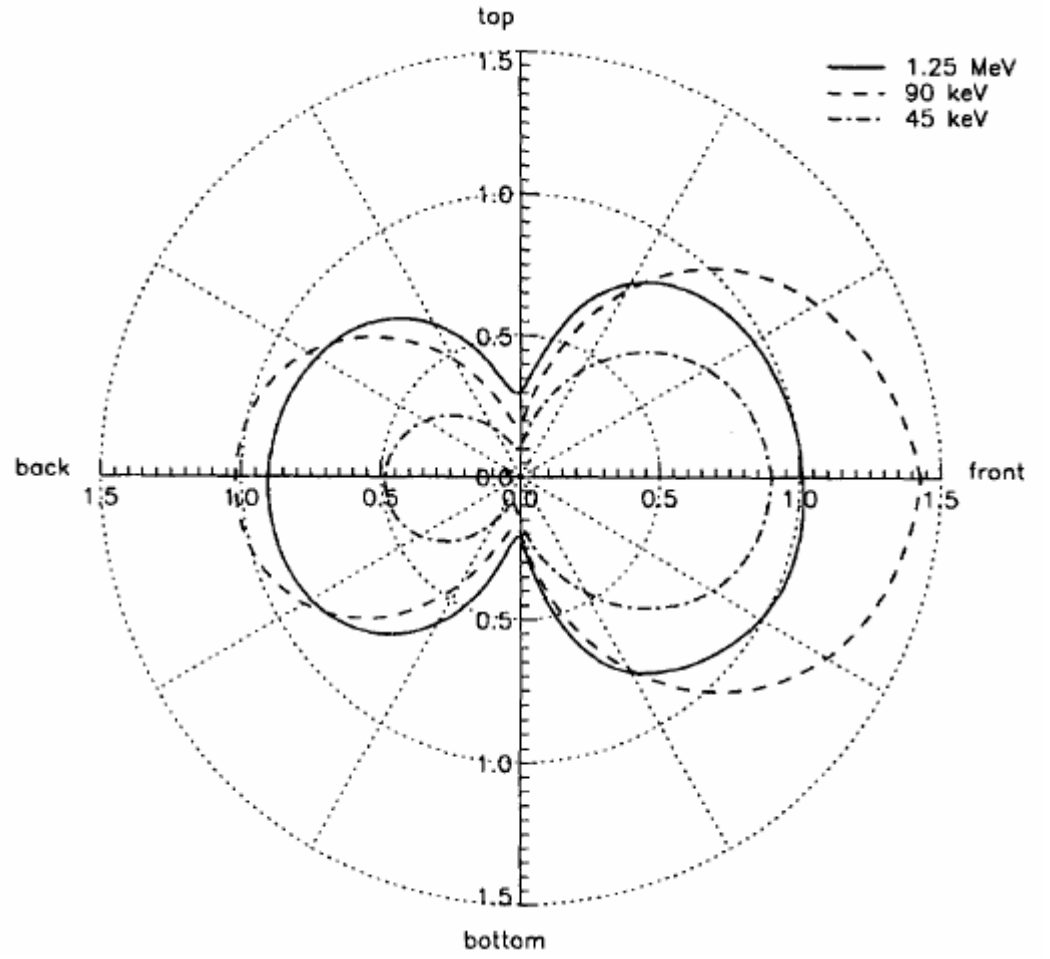

Figure 8: The angular variation of effective dose for photons; effective dose per unit air kerma in free air, E/K_a, for monoenergetic parallel photon beams incident at various angles on an adult anthropomorphic computational model (ICRP 1996).

With vertically varying incidence, one can see that the ICRP (1996) conversion coefficients increase in both the anterior and posterior positions (anterior is more pronounced) and decrease sharply when the angle is both proximal (top) and distal (bottom) to the exposed phantom. This sharp decrease is due to several factors such as asymmetrical organs, but is caused mostly by the increased shielding of organs by the

body. Applying a maximum angle of incidence of sixty degrees to Figure 8, one can estimate that the conversion coefficients for a 140 keV photon will vary from 1.3, 1.05, and 0.75 when the incident angle changes from zero, to thirty, and sixty degrees, respectively, as measured from the front towards the bottom. This would indicate that an arithmetic average response would be approximately 1.03 for all angles zero through sixty degrees inclusive.

II.3.c Randall-Wilkins Theory

A first-order kinetics approximation for escape of trapped charge carriers at a given temperature was first described by Randall and Wilkins in 1945 through the following equation (Attix 1986):

$$P = \frac{1}{\tau} = \alpha e^{-E/kT} \qquad \text{Eq.1}$$

where,

P is the probability of escape per unit time (s^{-1}),
τ is the mean lifetime in the trap,
α is called the frequency factor,
E is the energy depth of the trap (eV),
k is Boltzman's constant ($k=1.381 \times 10^{-23}$ J K^{-1}),
T is temperature in Kelvin.

Inspection of this equation would lead one to assume that if k, E, and α are held constant, increasing T will cause P to increase and τ to decrease. In more meaningful terms, this implies that, for a constant incident radiation energy and frequency factor, an increase in temperature applied to the TLD will result in an increase in the probability that an electron will escape back into the conduction band, recombine with a thermoluminescence center, and release visible light photons.

It follows that if one increases the temperature linearly as a function of time, the

escape rate of trapped electrons will increase and reach a maximum release rate based on some maximum temperature. If it is further assumed that the intensity of the light emission is proportional to the electron escape rate, a corresponding peak in thermoluminescence brightness will occur at the maximum temperature. This peak is called a “glow peak” and is shown in Figure 9.

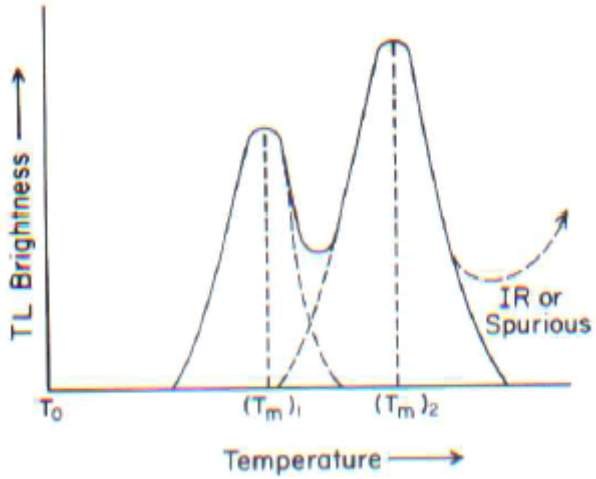

Figure 9: A thermoluminescence glow curve versus temperature (after Attix 1986).

The multiple peaks shown in the glow curve in Figure 9 are due to the thermoluminescence phosphor containing two different trap depths. The “IR” or “Spurious” markings are presented on the graph to indicate that a temperature greater than 300°C results in the infrared spectrum, produced by the heating element, contributing to the detected brightness of the glow curve. Generally, flowing an inert gas, such as nitrogen, into the TLD heating

area can reduce this occurrence, although in modern dosimetry systems, this phenomenon is of little significance.

II.3.d Trap Stability

If the traps are not stable at room temperature, as discussed in section II.3.b (4), they may migrate through the crystal structure and combine with other traps to form different configurations. TLD-100 exhibits this property to some extent. This problem is minimized by annealing the TLD prior to and after use. Another stability problem with TLDs is trap leakage. Trap leakage is the inability of the phosphor material to hold charge carriers at ambient temperatures after irradiation. Typically, the lower the temperature of the glow peak, the greater the effect of trap leakage after irradiation occurs (Attix 1986).

II.3.e Intrinsic Efficiency of TLD Phosphors

It should be noted that only a small portion of the energy deposited in a TLD phosphor is emitted as light when the phosphor is heated. The ratio of TL light energy emitted per unit mass compared to total deposited energy is called the intrinsic thermoluminescence efficiency. The intrinsic thermoluminescence efficiency of TLD-100 is about 0.039% (Attix 1986).

II.4 MCNP Simulation

Monte Carlo transport methods are very different from deterministic transport methods. Deterministic methods solve the transport equation for the average particle behavior and Monte Carlo methods simulate individual particles and record some aspects (tallies) of their average behavior (Briesmeister, 2000). The average behavior of particles in the experiments is inferred from the average behavior of the simulated particles. The details of how the MCNP code utilizes geometry cards, variance reduction techniques, tally

cards, cross section libraries, materials cards, particle tracking, and source definitions is discussed next.

II.4.a Tally Cards

Tally cards are used to specify what calculations the MCNP code will be instructed to perform. MCNP provides six standard neutron and photon tallies and four standard electron tallies (Briesmeister, 2000). The tallies used in this report averaged photon flux over a cell (F4 Tally) in units of particles cm^{-2}, and averaged energy deposition in a cell (F6 Tally) in units of MeV g^{-1}. Absorbed dose is expressed in the units of grays (Gy), where one Gy is equal to one joule kg^{-1}.

In MCNP, a cell represents a region of dosimetric interest. In the calculations described here, a cell does not necessarily represent an entire organ. Instead, several small volumes of each organ were used to tally the amount of energy deposited per gram of tissue in the tally volume using an F6 tally. The tally volumes used were two cm^3. The number of tallies for an individual organ was summed, an arithmetic average determined, and the average organ absorbed dose calculated. Applying a quality factor of one to absorbed dose due to the type of radiation received converts the absorbed dose (in Gy) to the dose equivalent in sieverts (Sv). The units of Gy and Sv are the same and neither of the tallies mentioned above could be used to calculate absorbed dose directly. Applying a fluence to dose conversion factor to the F4 tally converts the result from particles cm^{-2} to absorbed dose in rem. To conform to the SI Units System, the unit rem must be converted to the unit Sv and so the results from the F4 tally are divided by 100 since 1 Sv is equal to 100 rem. Applying a multiplier to convert MeV g^{-1} to J kg^{-1} and Gy to Sv provided the final tally results in units of Sv for the F6 tally.

II.4.b MCNP Geometry Definitions

MCNP version 4C comes equipped with various types of geometry specifications, tallies, materials definitions, source specifications, and variance reduction techniques. The geometry used in MCNP treats an arbitrary three-dimensional configuration of user-defined materials in geometric cells bounded by first- and second-degree surfaces and fourth-degree elliptical tori. The cells are defined by intersections, unions, and complements of the regions bounded by the surfaces and are treated in a Cartesian coordinate system. Surfaces are defined by supplying coefficients to the analytical surface equations, or for certain types of surfaces, known points on the surface. In the MCNP code, the operator has the added flexibility of defining geometrical regions from all the first- and second-degree surfaces of analytical geometry and elliptical tori and then combining them with Boolean operators.

II.4.c Materials Description Cards

The materials description cards in MCNP specify both the isotopic composition of the materials and the cross section evaluations to be used in the cells. The entries on the materials description cards are in the form of ZAID.nnX followed by the appropriate fraction of that particular element. In this expression, Z represents the atomic number of the element, A represents the mass number, ID is the identification that is added to make the Mnemonic ZAID, nn is the library identifier, and X is the class of data.

II.4.d Source Definition Card

A source definition card, SDEF, is one of four available methods of defining starting particles. The SDEF card defines the basic source parameters, such as position, starting cell number, starting energy, starting weight, starting time, and type of particle. If the user

wants to define a source other than a point isotropic source, then the Source Information (SI) and Source Probability (SP) cards should be used. The SI card defines either values of the source variable or some distribution numbers. Coupled to the SI card is the SP card. The SP card entries are probabilities that correspond to the entries on the SI card. In some cases, when long distances exist between the source particle and the target, a Source Bias (SB) card may be utilized. The SB card is used to provide a probability distribution for sampling that is different from the true probability distribution on the SP card. Its purpose is to bias the sampling of its source variable to improve the convergence rate of the problem. The weight of each source particle is adjusted to compensate for the bias.

II.4.e Variance Reduction Techniques

There are four classes of variance reduction techniques used in MCNP. The four classes are truncation methods, population control methods, modified sampling methods, and partially-deterministic methods. For the sake of brevity, only the *modified sampling method* technique used in this study will be discussed herein. Source biasing in MCNP, although not completely general, allows the production of more source particles, with appropriately reduced weights, in the more important regimes of each variable. Source directional biasing, used in this model, can be sampled from an exponential density function

$$p(\mu) = Ce^{K\mu}, \qquad \text{Eq. 2}$$

where,

$$C = \frac{K}{\left(e^{K} - e^{-K}\right)},$$

$\mu = \cos\theta$, where θ is the angle relative to the biasing direction.

K is typically equal to one and defines the ratio of weight of tracks starting in the biasing direction to tracks starting in the opposite direction. In this experiment, K=3.5 since this increases the amount of directional biasing towards the receptor. Thus, the ratio is equal to 1/1097, or 9.12 x10^{-4}.

II.4.f The Dispersal Model

The MCNP model was used to simulate the experimental dose measurements using the $Na^{99m}TcO_4$ radiation source. Figure 10 represents the experimental setup used in the study.

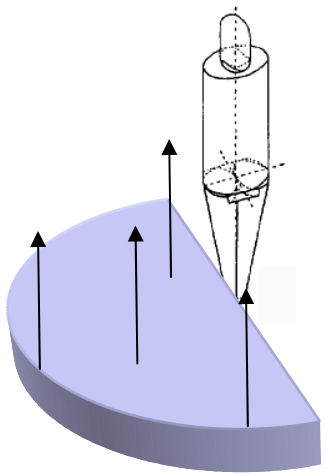

Figure 10: Inferior-superior ^{99m}Tc exposure geometry for the Rando® phantom.

The radius of the semi-circular geometry in Figure 10 was three meters and the region contained 360 liters of water, 71 liters of olive oil (with 55% to 80% oleic acid) and the $Na^{99m}TcO_4$ solution. The 360 liters of water allowed a water depth of 2.5 cm and the 71 liters of olive oil added another 0.5 cm. Ten mL of $Na^{99m}TcO_4$ solution containing an activity of 7.4 GBq of ^{99m}Tc was dispersed onto the oleic acid.

The geometry used in the MCNP model assumed that water was located on the bottom of the semi-circle as the first layer. This was followed by oleic acid on top of the water as the middle layer, and finally the $Na^{99m}TcO_4$ solution as the third and final layer. The materials cards used in the MCNP code described the water as H_2O with a density of 1.0 g cm^{-3}, the olive oil as pure oleic acid, $C_{18}H_{34}O_2$ with a density of 0.895 g cm^{-3}, and the $Na^{99m}TcO_4$ solution contained a total of 2.3×10^{14} atoms of ^{99m}Tc. To account for scatter of the ^{99m}Tc gamma rays, the MCNP model also included the concrete floors, walls, and ceiling. Figure 11 below shows the geometry used in the MCNP model calculation. The room was 7m wide by 25m long, one meter thick concrete walls, and 5m high ceiling.

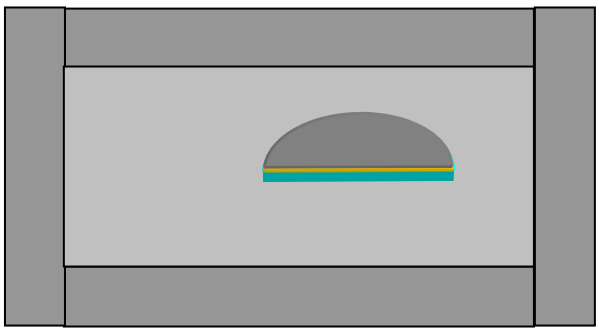

Figure 11: MCNP model depicting layered water, olive oil, and $Na^{99m}TcO_4$ and room barriers.

II.4.g The Phantom Model

The MCNP software can be used to simulate the human body through use of various geometry and material cards available as a standard feature of the software package. The MCNP user's manual covers the technical use and description of the materials and geometry cards discussed in section II.4.b. Since simulation of the human body is complex and time consuming, the amount of computing time can be intensive because particle tracking must occur through a variety of surfaces. All tissues and organs used in this simulation derived their descriptions from the ICRP (1975). As an additional aid, a software package known as Body Builder† was used to model the Rando® phantom and respective organs. This software was used to provide an MCNP-based description of an age and sex-specific human body for use as an input to the MCNP transport code. In this investigation, an adult male described as "The Reference Man" by ICRP (1975) was modeled. Figure 12 shows the internal structure of the model.

† White Rock Science, P.O. Box 729 White Rock, NM 87544, 505-672-1105.

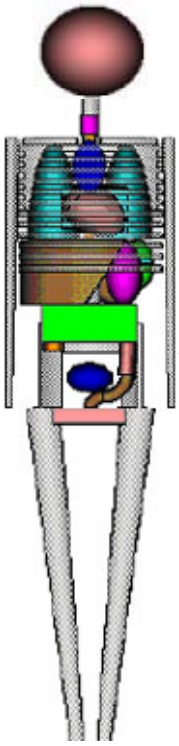

Figure 12: MCNP modeled adult male human body.

Although arms are included in Figure 12, the arms were “commented out” during the MCNP simulations. That is, the arms were not simulated and, thus, no particle interaction or tracking occurred during the computer simulations. This choice was made due to the use of the Rando® phantom. The phantom did not have arms during the experimental process and so, in an attempt to construct as representative a model as possible, the arms were not simulated. The Rando® phantom did not have legs either, so the experimental setup used planks of wood to simulate legs. This also provided a means to mount the phantom at the proper height above the planar source.

III. MATERIALS AND METHODS

III.1 Preparation of the Source Geometry

The semi-circular geometry needed for the investigation was constructed by using 4-mil plastic sheeting,‡ laminate plastic moulding track[§] to have the plastic retain the semi-circular shape needed, and binder clips[**] to hold the plastic sheeting to the plastic moulding. The semi-circle source geometry was constructed in the basement of the Zachry Engineering Center at Texas A&M University in an area where ingress and egress could be closely monitored and only those personnel involved in the investigation could enter.

After assembly of the plastic sheeting and moulding track, water was carefully applied over the surface of the plastic and provided a 2.5 cm thick hydrophilic binding surface for the 0.5 cm thick olive oil (containing the oleic acid).

III.2 Preparation of the Rando® Phantom

After constructing the irradiation source geometry, the Rando® phantom was moved into place, as shown in Figure 10 of section II.4.f of this report. Figure 13 is a photograph of the Rando® phantom used in this investigation. Note that the phantom is transected-horizontally, where each slice is 2.5 cm thick.

---

‡ Manufactured by Frost King – Thermwell Products Company, Inc., 420 Route 17 South Mahwah, NJ 07430 Model Number P1014.

§ Shaw Industries, Inc. P.O. Drawer 2128 616 E. Walnut Avenue Dalton, GA 30722-2128

** OfficeMax Corporate Headquarters 150 E. Pierce Road Itasca, IL 60143 Item # 20168809

Figure 13: Photograph of the Rando® phantom.

The segments of the phantom are printed with a unique identifier number on the anterior portion of the phantom and the slices used in this investigation ranged from slice number 16 to 31, which contained organs from the top of the lungs down to the colon on the right side of the phantom. Each slice contained a unique numbering system with holes created specifically for TLD placement; where the size of each hole was 0.8 cm x 0.8 cm diameter and the distance between holes was on a 3.0 cm x 3.0 cm grid. Where TLDs were not used, bone equivalent, tissue equivalent, or lung equivalent plugs, as appropriate,

were used to fill in unused holes. Table 1 provides an example of the numbering convention imprinted on each slice of the phantom. In this Table grid A1 represents the right posterior portion of the phantom (e.g., an area where a kidney might be located).

Table 1: Phantom numbering convention for TLD placement per slice.

A1	A2	A3	A4	A5	A6	A7
B1	B2	B3	B4	B5	B6	B7
C1	C2	C3	C4	C5	C6	C7
D1	D2	D3	D4	D5	D6	D7
E1	E2	E3	E4	E5	E6	E7
F1	F2	F3	F4	F5	F6	F7

Appendix A contains thirty-two tables indicative of the placement of each TLD in its respective location. TLDs used inside the phantom throughout this investigation were DXT-RAD dosimeters (TLD-100) manufactured and distributed by Thermo Electron Corporation[††] . Each TLD contained a permanent, identification barcode to allow tracking

†† Thermo Electron Corp. contact Mike Shepherd in Duluth, GA Tel: 770-335-7699

in addition to the matrix type of number convention provided with the phantom. The absorbed doses were measured in the following organs:

- Small Intestine
- Kidney
- Liver
- Ascending Colon
- Transverse Colon
- Gall Bladder
- Pancreas
- Right Lung

After placement of all DXT-RAD dosimeters, four Panasonic model UD-802A TLD packages were placed on the exterior of the phantom. A TLD was placed on the center torso of the phantom in the anterior (AP), posterior (PA), left lateral (LLAT), and right lateral (RLAT) positions. Table 2 provides a description of the Panasonic UD-802A TLD package.

Table 2: Panasonic UD-802 TLD package description.

		Element 1	Element 2	Element 3	Element 4
UD-802A	Phosphor	$Li_2B_4O_7$	$Li_2B_4O_7$	$CaSO_4$	$CaSO_4$
	Front Filtration	Plastic 14 mg cm^{-2}	Plastic 160 mg cm^{-2}	Plastic 160 mg cm^{-2}	Lead 0.7 mm
	Rear Filtration	Plastic 14 mg cm^{-2}	Plastic 160 mg cm^{-2}	Plastic 160 mg cm^{-2}	Lead 0.7 mm

III.3 Basis for the Selection of Sodium Pertechnetate

During the initial planning to establish a suitable geometry for exposing the Rando® phantom, concern for uniformly distributing a radionuclide over the surface of a suitable substrate led to the conclusion that an aqueous solution would likely provide the best result. The selection of $Na^{99m}TcO_4$ provided a solution for meeting this research criterion. The criteria for selection of a particular radionuclide are listed below.

- Easy to manufacture in moderate to large quantities
- Ease of transportation and dispersion
- Moderate to low cost
- Short radioactive half-life
- Ease of measurement
- Common radionuclide
- Made in liquid form (to enhance dispersion)

Early during the design of the exposure geometry, the use of concrete, wood, steel, or plastic substrates on which to disperse the $Na^{99m}TcO_4$, presented some minor challenges. Overcoming non-uniform distribution of the $Na^{99m}TcO_4$ due to surface tension difficulties of the liquid presented the largest of the hurdles. Surface tension of liquids on the substrate impeded the ability of the liquid to smoothly move from one location to another uninhibited. This inhibition would have eventually led to large errors in the uniform distribution of the radionuclide over the surface of the substrate and, thus, present a non-uniform exposure geometry. Moreover, the use of these common materials made radioactive waste generation a major concern, which would subsequently lead to larger waste volumes and become cost-prohibitive because of the additional effort required to purchase waste containers needed to store the waste.

Since $Na^{99m}TcO_4$ is water soluble, the question of uniform distribution of the radionuclide changed to one of whether a non-water soluble substance could be used to help distribute the water soluble $Na^{99m}TcO_4$. Research efforts revealed that oleic acid

provided such a solution.

III.4 Basis for the Selection of Oleic Acid

Like many fatty acids, oleic acid has both a hydrophilic (water attractive) head and a hydrophobic (water repulsive) tail. More precisely, oleic acid is an eighteen carbon molecule that possesses only one double bond in its hydrocarbon sequence and thus is also known as a monounsaturated fatty acid. Oleic acid is a naturally occurring fatty acid and is most abundant in olive oil. Olive oil contains approximately 55% to 80% oleic acid (Brown 1995).

Given that the $Na^{99m}TcO_4$ is an aqueous, isotonic saline solution, it makes intuitive sense that the hydrophobic tail of the oleic acid will serve to repel the $Na^{99m}TcO_4$ while the hydrophilic head will be attracted to the 2.5 cm-thick layer of water. In this manner, if the olive oil is resting on top of a thin layer of water due to the hydrophilic head being oriented towards the water, then the hydrophobic tail will be oriented upwards and away from the water. Subsequent application of the $Na^{99m}TcO_4$ solution will be repelled by the hydrophobic tail and the material will be spread uniformly across the surface of the olive oil.

III.5 Delivery of the $Na^{99m}TcO_4$

The addition of the $Na^{99m}TcO_4$ to the semi-circular geometry occurred in two phases of each monitoring period. There were initially three monitoring periods for this investigation, but the data from the first monitoring period was disregarded since the phantom assembly inexplicably fell over during the evening portion of the exposure causing three of the DXT-RAD dosimeters to become damaged and the remaining dosimeters found lying in the water, olive oil, and $Na^{99m}TcO_4$. A monitoring period was defined as one in which the total exposure of the TLDs to the penetrating radiation from the $Na^{99m}TcO_4$

solution lasted for twenty-four hours. There were two subsequent monitoring periods and during each of these monitoring periods, there were two additions of a 10 mL $Na^{99m}TcO_4$ solution; where each solution contained 7.4 GBq of ^{99m}Tc.

Each addition of $Na^{99m}TcO_4$ was accomplished by extracting the 10 mL volume from a glass vial and injecting the volume onto the surface of the oleic acid. As an added precaution, anti-contamination clothing was worn. Mechanical agitation of the water and oleic acid ensured uniform distribution of the $Na^{99m}TcO_4$. The $Na^{99m}TcO_4$ additions during the monitoring period were administered at 0800 Central Standard Time (CST) and at 1400 CST.

Personnel conducting the experiments periodically entered and exited the exposure area to document exposure parameters. From 0800 CST to 2000 CST, radiation measurements with the Victoreen Model 450P ionization chamber were conducted every four hours. In addition to collecting dose rate information using the Victoreen 450P, integrated dose information was also obtained since this instrument could provide dose rate and integrated dose during the entire monitoring period. The results of the radiation measurements are contained in Appendix B. The integrated dose measurements from the Victoreen 450P were used for comparison to dosimeter results as would normally be conducted in a practical field exercise. At the end of each monitoring period, the DXT-RAD dosimeters and the TLD packages were removed from the phantom and shipped to the US Air Force Radiation Dosimetry Branch at Brooks City-Base, Texas where the TLDs were evaluated and results recorded.

At the conclusion of the final monitoring period, approximately 115 kg of vermiculite was needed to absorb the entire volume of water, olive oil, and residual $Na^{99m}TcO_4$. The waste was packaged in strong, tight containers, labeled as radioactive material and allowed

to decay. Once the appropriate decay time had passed, the Texas A&M University Environmental, Health, and Safety Department was contacted so their radiological technicians could transport the waste to a storage area to await final disposition.

III.6 Full Circle MCNP Simulation

After completing model validation, a full three-meter radius circle simulation was conducted. This simulation should provide more useful results applicable to a scenario involving gamma-emitting radionuclides. In general, the estimation methods can be scaled according to the amount of radioactivity present. That is, if the amount of radioactivity present in a second event is twice that of the hypothetical event described here, then one may expect a two-fold increase in effective dose and organ absorbed dose. Using MCNP, a full circle model simulation was conducted assuming a source of 29.6 GBq.

IV. RESULTS

IV.1 DXT-RAD Dosimeter Results

Exactly 128 DXT-RAD dosimeters were used in each of the exposures. The measured values and the MCNP-calculated results are presented in Tables 3 and 4. Calculated results in Tables 3 and 4 are from a single MCNP calculation. Specific DXT-RAD dosimeter results can be found in Appendix C for each organ for each monitoring period. There were several DXT-RAD dosimeters assigned to each organ and their position inside the organ attempted to take into account the non-uniformity of the absorbed dose across the whole organ. Non-uniformity of the absorbed dose is present since the organ tissue will attenuate the number of photons entering the organ. As tissue depth increases, then the number of photons available for interaction decrease exponentially. All individual DXT-RAD dosimeter results assigned to each organ were averaged. The results were not corrected for energy and angular dependent responses. The average absorbed dose to the following organs was measured with the DXT-RAD dosimeters and modeled using MCNP:

- Small Intestine
- Kidney
- Liver
- Ascending Colon
- Transverse Colon
- Gall Bladder
- Pancreas
- Right Lung

Table 3: Organ absorbed dose for monitoring periods 1 and 2, uncorrected for energy and angular dependence.

Organ	Monitoring Period 1		Monitoring Period 2	
	Measured Results[1,2] (mGy)	Calculated Results[3] (mGy)	Measured Results[1,2] (mGy)	Calculated Results[3] (mGy)
Small Intestine	1.02 ± 0.24	0.85 ± 0.06	1.03 ± 0.12	0.85 ± 0.06
Kidney	0.79 ± 0.10	0.67 ± 0.05	0.82 ± 0.11	0.67 ± 0.05
Liver	0.97 ± 0.24	0.82 ± 0.06	1.01 ± 0.26	0.82 ± 0.06
Ascending Colon	1.04 ± 0.18	0.86 ± 0.07	1.13 ± 0.22	0.86 ± 0.07
Transverse Colon	0.83 ± 0.13	0.68 ± 0.04	0.87 ± 0.18	0.68 ± 0.04
Gall Bladder	0.90 ± 0.11	0.73 ± 0.03	1.01 ± 0.10	0.73 ± 0.03
Pancreas	0.75 ± 0.11	0.62 ± 0.06	0.76 ± 0.12	0.62 ± 0.06
Right Lung	0.85 ± 0.17	0.70 ± 0.04	0.88 ± 0.18	0.70 ± 0.04

1) Results are rounded up to the nearest one-hundredth.
2) The error expressed in these measurements is the overall system error and is calculated as the square root of the sum of the squares of the individual results' standard deviation and measurement error, per guidance in NCRP Report 58.
3) Error in these calculated results is expressed as relative error; MCNP defines relative error, $R = \sigma / \bar{x}$, where σ is the standard deviation of the mean and $\bar{x}$ is the mean.

Recall from section II.3.b (5) and II.3.b (6) that the DXT-RAD dosimeters respond differently depending upon the photon energy and the angle of incidence between the photon and dosimeter. Data in section II.4.a (5) indicate LiF TLD material will over-respond by a factor of 1.08 when exposed to 140.5 keV photons. Similarly, in section II.3.b (6), LiF TLD material will over-respond by a factor of 1.03 when exposed to 140 keV photons at an angle of zero to sixty degrees. Considering both sources of over-

response, the DXT-RAD dosimeters will over respond by about 11%. Hence, all measured values were divided by a factor of 1.11 to account for this over-response. Table 4 shows the results of correcting for the over-response.

Table 4: Organ absorbed dose for monitoring periods 1 and 2, corrected for energy and angular dependence.

Organ	Monitoring Period 1		Monitoring Period 2	
	Measured Results[1,2] (mGy)	Calculated Results[3] (mGy)	Measured Results[1,2] (mGy)	Calculated Results[3] (mGy)
Small Intestine	0.92 ± 0.24	0.85 ± 0.06	0.93 ± 0.19	0.85 ± 0.06
Kidney	0.72 ± 0.10	0.67 ± 0.05	0.74 ± 0.11	0.67 ± 0.05
Liver	0.87 ± 0.24	0.82 ± 0.06	0.91 ± 0.26	0.82 ± 0.06
Ascending Colon	0.93 ± 0.18	0.86 ± 0.07	1.02 ± 0.22	0.86 ± 0.07
Transverse Colon	0.75 ± 0.13	0.68 ± 0.04	0.78 ± 0.18	0.68 ± 0.04
Gall Bladder	0.81 ± 0.11	0.73 ± 0.03	0.91 ± 0.10	0.73 ± 0.03
Pancreas	0.68 ± 0.11	0.62 ± 0.06	0.69 ± 0.12	0.62 ± 0.06
Right Lung	0.76 ± 0.17	0.70 ± 0.04	0.79 ± 0.18	0.70 ± 0.04

1) Results are rounded up to the nearest one-hundredth.
2) The error expressed in these measurements is the overall system error and is calculated as the square root of the sum of the squares of the individual results' standard deviation and measurement error, per guidance in NCRP Report 58.
3) Error in these calculated results is expressed as relative error; MCNP defines relative error, $R = \sigma / \bar{x}$, where σ is the standard deviation of the mean and $\bar{x}$ is the mean.

Since tabular data do not provide adequate scaling for comparison purposes, a graphical representation of the data for both monitoring periods is provided in Figures 14 and 15.

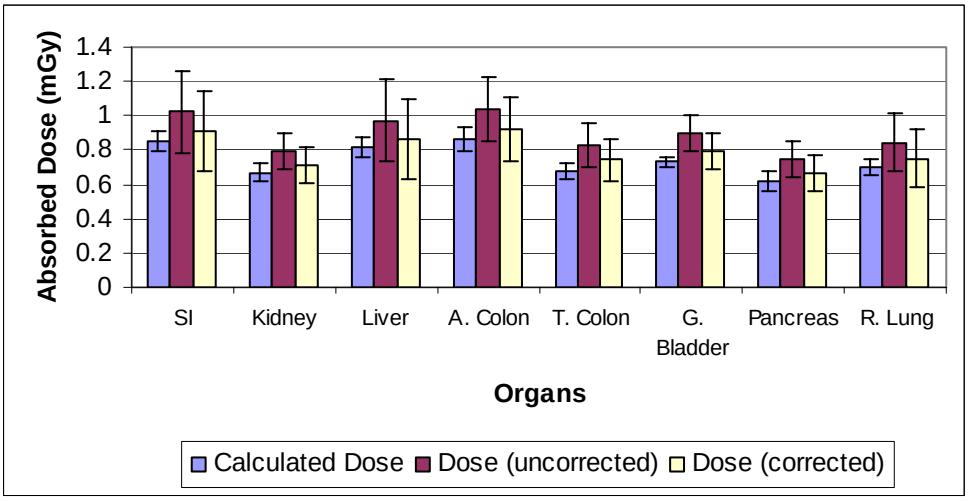

Figure 14: Monitoring period number one, organ-specific absorbed dose results.

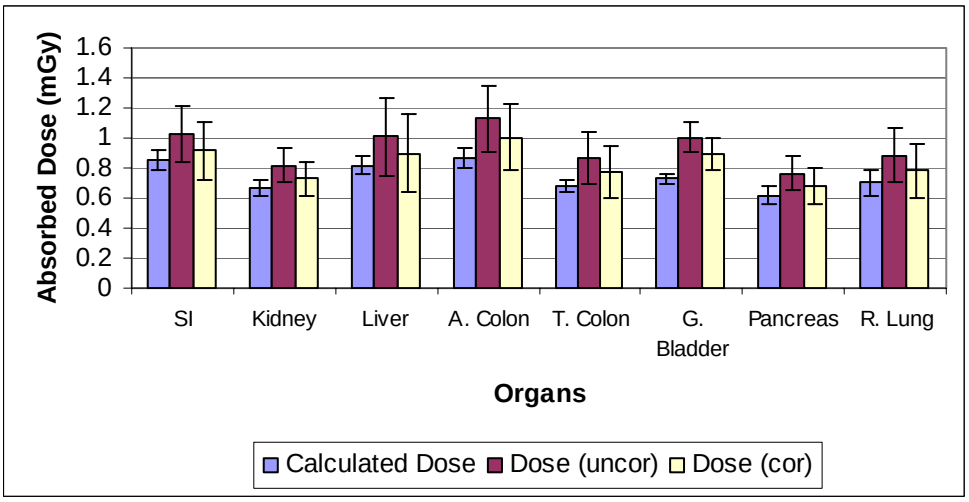

Figure 15: Monitoring period number two, organ-specific absorbed dose results.

IV.2 Panasonic UD-802A TLD Results

Four Panasonic UD-802A TLDs were used for each of the monitoring periods. Measured results for both monitoring periods are presented in Table 5. In this study, only the "deep" values were used. The results are expressed in units of mSv and are automatically corrected for energy and angular dependent responses at the time the dosimeters are processed. This automatic correction is accomplished at the US Air Force Radiation Dosimetry Branch by simulating the angular distribution observed in this investigation at the Air Force dosimetry laboratory. The simulated angles are provided as input to the algorithm that reports absorbed dose. In addition, the US Air Force reports a uniform $\pm$ 10% error for all TLD results[‡‡].

[‡‡] Personal communications with Mike Klueber at the US Air Force Radiation Dosimetry Branch.

Table 5: Panasonic UD-802 TLD results.

Whole Body Dosimeter Results (mSv)					
Badge ID	Shallow	Eye	Deep	Position	Monitoring Period
301977	0.62 ± 0.06	0.65 ± 0.07	0.65 ± 0.07	AP	1
301972	0.54 ± 0.05	0.57 ± 0.06	0.57 ± 0.06	PA	1
301971	1.08 ± 0.11	1.12 ± 0.11	1.12 ± 0.11	RLAT	1
301978	0.23 ± 0.02	0.24 ± 0.02	0.24 ± 0.02	LLAT	1
301970	0.72 ± 0.07	0.73 ± 0.07	0.73 ± 0.07	AP	2
301973	0.56 ± 0.06	0.58 ± 0.06	0.58 ± 0.06	PA	2
301968	1.17 ± 0.12	1.23 ± 0.12	1.23 ± 0.12	RLAT	2
301976	0.3 ± 0.03	0.31 ± 0.03	0.31 ± 0.03	LLAT	2

The organ-absorbed dose results have little meaning when attempting a comparison with values for the Panasonic TLD results. Modifying factors need to be applied, so that the results of the DXT-RAD dosimeters can be compared to the results of the Panasonic TLDs. ICRP Report No. 74 (1996) discusses conversion of an operational quantity known as the personal dose equivalent, $H_P(10)$, to free-in-air kerma, K_a. Table A.24 in ICRP Report No. 74 (1996) provides energy-dependent conversion coefficients for this process and for a 140.5 keV photon, the conversion coefficient is 1.643 ($H_P(10)/K_a$, in units of Gy/Gy). Now that free-in-air kerma is available, one only need interpolate an energy-dependent conversion coefficient for a specific organ from ICRP Report No. 74 (1996) to convert K_a into absorbed dose, D_T.

The conversion coefficients are organ specific because of different tissue compositions, location within the body, and shielding effects from other organs. The following conversion coefficients were used:

- SI – 0.876
- Kidney – 0.876
- Liver – 0.901
- Ascending Colon – 0.855
- Transverse Colon – 0.855
- Gall Bladder – 0.876
- Pancreas – 0.876
- Right Lung – 0.952

Potentially, the absence of arms on the phantom resulted in higher absorbed doses for the individual organs. The absence of arms did not significantly affect the AP TLD, however. Therefore, taking a ratio of the RLAT TLD compared to the AP TLD provided an adequate method to determine the factor by which all measured organ absorbed dose results should be adjusted. Taking this ratio shows that the RLAT TLD is approximately a factor of 1.72 higher than the AP TLD. Consequently, all energy and angular-corrected organ absorbed doses need to be divided by a factor of 1.72 before comparing their values to those derived from the use of organ-specific conversion coefficients.

Tables 6 and 7 provide the results obtained after applying the conversion coefficients to the AP Panasonic TLD and dividing all energy and angular-dependent organ absorbed dose results by a factor of 1.72.

Table 6: Organ absorbed doses derived from Panasonic UD-802 TLDs compared to DXT-RAD dosimeters.

Organ	Monitoring Period 1	
	DXT Absorbed Dose after a 1.72 reduction factor[1] (mGy)	Panasonic Results after using Conversion Coefficients (mGy)
Small Intestine	0.53 ± 0.14	0.35 ± 0.04
Kidney	0.41 ± 0.06	0.35 ± 0.04
Liver	0.50 ± 0.14	0.36 ± 0.04
Colon (averaged)	0.48 ± 0.09	0.34 ± 0.03
Gall Bladder	0.47 ± 0.06	0.35 ± 0.04
Pancreas	0.39 ± 0.06	0.35 ± 0.04
Right Lung	0.44 ± 0.10	0.38 ± 0.04

1) Overall system error is calculated as the square root of the sum of the squares of the standard deviation and measurement error, per guidance in NCRP Report 58. Effective doses calculated from radiation and tissue weighting factors provided by ICRP (1991).
2) Note that ICRP (1996) conversion coefficients have been applied.

Table 7: Organ absorbed doses derived from Panasonic UD-802 TLDs compared to DXT-RAD dosimeters.

Organ	Monitoring Period 2	
	DXT Absorbed Dose after a 1.72 reduction factor[1] (mGy)	Panasonic Results after using Conversion Coefficients (mGy)
Small Intestine	0.53 ± 0.11	0.35 ± 0.04
Kidney	0.42 ± 0.06	0.35 ± 0.04
Liver	0.52 ± 0.15	0.36 ± 0.04
Colon (averaged)	0.52 ± 0.12	0.34 ± 0.03
Gall Bladder	0.52 ± 0.06	0.35 ± 0.04
Pancreas	0.40 ± 0.07	0.35 ± 0.04
Right Lung	0.45 ± 0.10	0.38 ± 0.04

1) Overall system error is calculated as the square root of the sum of the squares of the standard deviation and measurement error, per guidance in NCRP Report 58. Effective doses calculated from radiation and tissue weighting factors provided by ICRP (1991).
2) Note that ICRP (1996) conversion coefficients have been applied.

Again, since tabular data do not provide adequate scaling for comparison purposes, graphical representations of the data for both monitoring periods are provided in Figures 16 and 17.

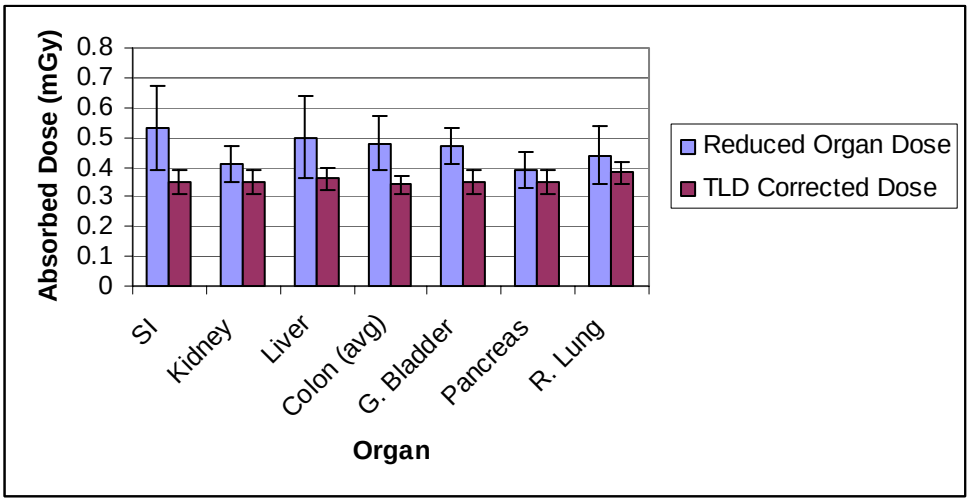

Figure 16: Graphical representation of the data from Table 7.

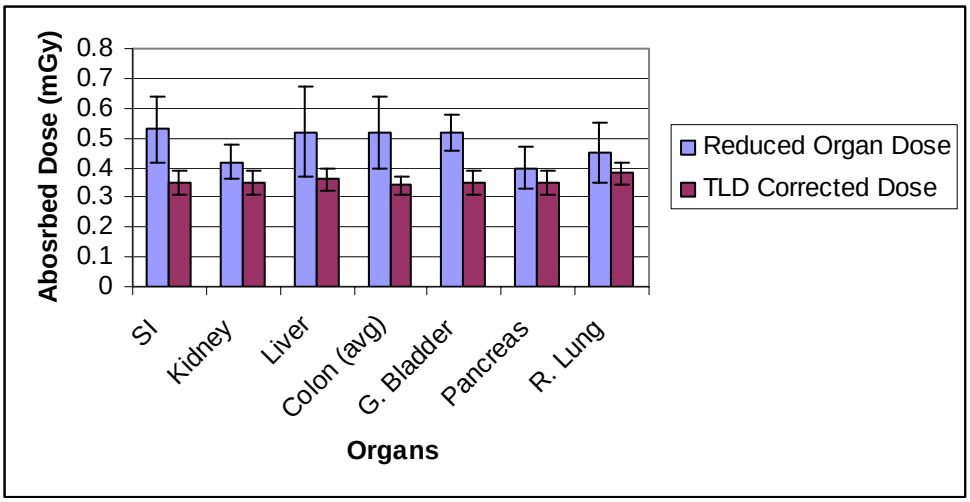

Figure 17: Graphical representation of the data from Table 8.

IV.3 Full Circle Modeling Results

Since the half-circle model produced acceptable, reproducible agreement between measured and calculated results, the MCNP model was considered to be validated. Extension of logic indicates that an MCNP simulation of a full-circle source provides more useful information when applied to a field condition such as an actual radiological emergency response. In this instance, the full circle source was assumed to represent an analogue to the ROT geometry; a geometry that is very likely to occur in an actual RDD scenario. The results of the MCNP simulation are presented in Table 8 along with derived organ-absorbed dose results converted from personal dose equivalent values from a simulated AP TLD. As described in section IV.2, conversion coefficients are required to convert effective dose to absorbed dose. So that the results of the absorbed dose can be compared to the results of the effective dose, modifying factors need to be applied. As previously discussed, Table A.24 in ICRP Report No. 74 (1996) provides energy-dependent conversion coefficients for converting effective dose into free-in-air kerma for a 140.5 keV photon and its value is 1.643 ($H_P(10)/K_a$, units of Gy/Gy). Now that free-in-air kerma is available, one only need interpolate an energy-dependent conversion coefficient for a specific organ from ICRP Report No. 74 (1996) to convert K_a into absorbed dose, D_T.

The conversion coefficients are organ specific because of different tissue compositions, location within the body, and shielding effects from other organs and the following coefficients apply:

- SI – 0.876
- Kidney – 0.876
- Liver – 0.901
- Ascending Colon – 0.855
- Transverse Colon – 0.855
- Descending Colon – 0.855
- Gall Bladder – 0.876
- Pancreas – 0.876
- Right Lung – 0.952
- Left Lung – 0.952
- Stomach – 0.891
- Bladder – 0.856
- Spleen – 0.876
- Heart – 0.876
- Thyroid – 1.174

The conversion coefficients for the SI, kidney, gall bladder, pancreas, spleen, and heart are all the same because they are considered to be remainder organs by ICRP (1996).

Table 8: MCNP results for the full disk simulation.

MCNP Full Circle Simulation Results			
Organ	Organ Absorbed Dose after a 24-hour exposure to 29.6 GBq (0.8 Ci) of ^{99m}Tc[1] (mGy)	Derived Organ Absorbed Dose from the AP TLD Effective Dose[3] (mGy)	Simulated AP TLD Effective Dose Results (mSv)[2]
Bladder	0.86 ± 0.09	0.70 ± 0.12	1.35 ± 0.12
Small Intestine	0.99 ± 0.15	0.72 ± 0.12	
Right Kidney	0.76 ± 0.09	0.72 ± 0.12	
Left Kidney	0.76 ± 0.09	0.72 ± 0.12	
Liver	0.87 ± 0.08	0.74 ± 0.12	
Colon (averaged)	0.97 ± 0.11	0.70 ± 0.12	
Gall Bladder	0.92 ± 0.12	0.72 ± 0.12	
Pancreas	0.72 ± 0.08	0.72 ± 0.12	
Spleen	0.94 ± 0.13	0.72 ± 0.12	
Stomach	0.90 ± 0.09	0.73 ± 0.12	
Heart	0.85 ± 0.10	0.72 ± 0.12	
Right Lung	0.82 ± 0.08	0.78 ± 0.12	
Left Lung	0.82 ± 0.08	0.78 ± 0.12	
Thyroid	1.14 ± 0.11	0.96 ± 0.12	

1) GBq is gigabequerels, where 37 gigabequerels is equal to one curie. Overall system error is calculated as the square root of the sum of the squares of the standard deviation and measurement error, per guidance in NCRP Report 58. Effective doses calculated from radiation and tissue weighting factors provided by ICRP (1991).

2) Error in these calculated results are expressed as relative error; MCNP defines relative error, $R = \sigma / \bar{x}$, where σ is the standard deviation of the mean and $\bar{x}$ is the mean.

3) Since error is not reported with conversion coefficients in ICRP (1996), conversion coefficients are considered to be "constants" and thus carry no associated error. Therefore, total error is equal to the error to the results calculated by MCNP in note 2 above.

A graphical representation of the data for both monitoring periods is provided in Figure 18.

Note that the data are provided in columnar format with error bars for all data sets.

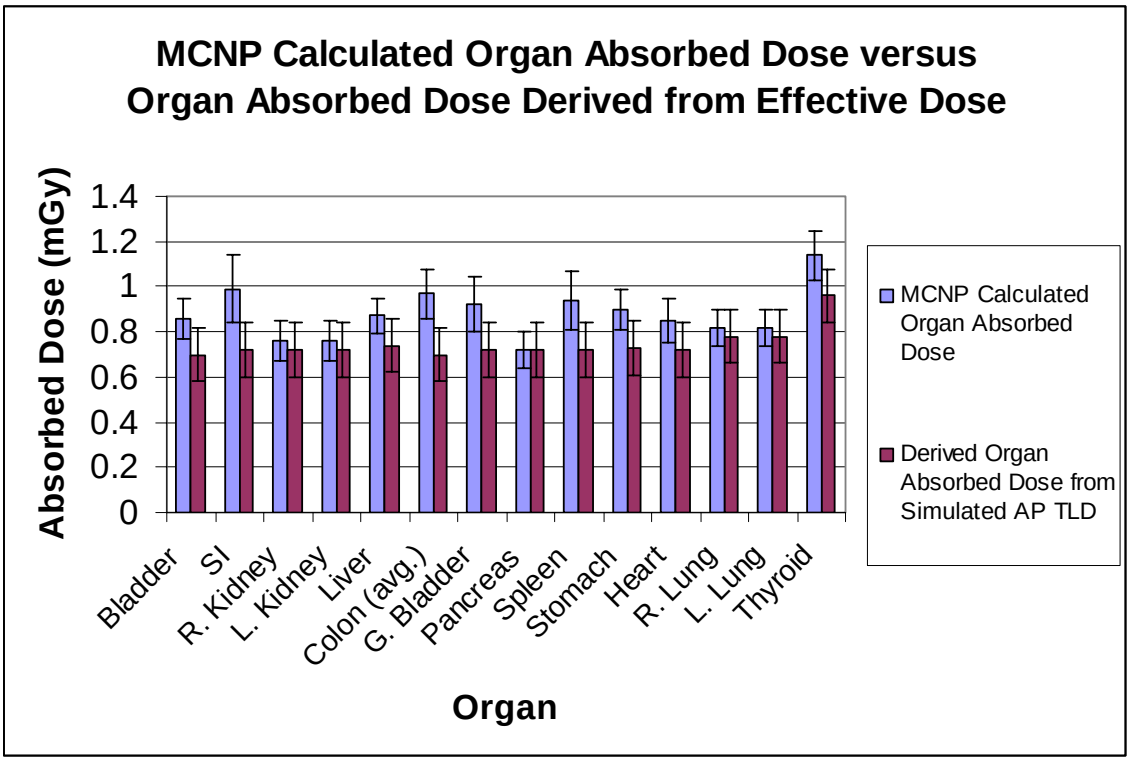

Figure 18: Graphical representation of the data fromTable 9.

An estimator that can be inferred from the data above is that in a 24-hour exposure period, there are 4.86×10^{-11} mSv Bq^{-1} (0.18 mrem mCi^{-1}) of $Na^{99m}TcO_4$ in a 3-meter radius circle geometry. This is calculated by dividing the simulated AP TLD value (1.35 mSv) by the total amount of radioactivity (29.6 GBq) used in the investigation. The estimator derived here is intended to provide estimated dose based upon the amount of radioactivity present, or conversely provide an estimate of the amount of radioactivity present based upon the dose received by the recipient.

IV.4 Radiological Monitoring Results

The instrumentation used to conduct radiation area monitoring was the Victoreen Model 450P (dose and dose rate). The results of the dose and dose rate information for both monitoring periods are provided in Tables 9 and 10.

Table 9: Victoreen 450P dose rate and integrated dose measurements for monitoring period number one.

Radiological Monitoring Parameters[1]		
Time (hours)	Dose Rate (mSv h^{-1})	Integrated Dose (mSv)
0	0.073 ± 0.015	0
4	0.05 ± 0.01	0.28 ± 0.06
8[2]	0.085 ± 0.017	0.6 ± 0.12
12	0.055 ± 0.01	0.85 ± 0.17
24	0.015 ± 0.003	1.17 ± 0.23

1) Results are provided with a uniform error of $\pm$ 20% as per the manufacturer's calibration procedures.
2) Another 7.4 GBq (200 mCi) of $Na^{99m}TcO_4$ added.

Table 10: Victoreen 450P dose rate and integrated dose measurements for monitoring period number two.

Radiological Monitoring Parameters[1]		
Time	Dose Rate ($mSv\ h^{-1}$)	Integrated Dose (mSv)
0	0.08 ± 0.016	0
4	0.052 ± 0.010	0.32 ± 0.06
8[2]	0.095 ± 0.019	0.68 ± 0.14
12	0.062 ± 0.012	0.95 ± 0.19
24	0.017 ± 0.003	1.3 ± 0.26

1) Results are provided with a uniform error of $\pm$ 20% as per the manufacturer's calibration procedures.
2) Another 7.4 GBq (200 mCi) of $Na^{99m}TcO_4$ added.

V. DISCUSSION

V.1 Comparison of Energy and Angular Corrected Values Versus Non-Corrected Values

An inspection of Figures 14 and 15 from section IV.1 reveals that energy and angular corrected measured values compare favorably with the calculated results from the MCNP modeling. One will want to note the significance of, or rather consequences of, not correcting for energy and angular dependence, however. A detailed review of the tabulated results in Table 3 of section IV.1 and a visual review of the graphs in Figures 14 and 15 indicate that several values, not corrected for energy and angular dependence, do not track well with the calculated values. Specifically, the lower end of the margins of error for the kidney, transverse colon, gall bladder, and pancreas uncorrected for energy and angular dependence do not compare favorably with the higher end margins of error for the calculated results. This observation indicates error is introduced when corrections for energy and angular dependence are not taken into account. In this instance, the consequence of not correcting for energy and angular dependent responses is that the observed values are over-estimated by a factor of 1.11. The MCNP model, however, does make this adjustment and the result is that lower-than-measured values are predicted. Moreover, an experimenter will most certainly need to know the energy of the incident photons, as well as the geometry of the source term to make appropriate corrections for energy and angular dependence. In a practical field exercise or actual deployment of an RDD/IND, the range of corrections values for energy and angular dependence needs to be known so that an order of magnitude assumption can be made by the IC.

V.2 Model Validation

The results presented in Table 5 of section IV.1 provide DXT-RAD measured organ-absorbed dose results that are corrected for energy and angular dependence. Table 4 also presents MCNP-calculated organ-absorbed dose results. Using Figures 14 and 15 to visually compare these results confirms that DXT-RAD measured results compare favorably to MCNP calculated results. Therefore, the MCNP model is assumed to be validated.

V.3 Verification of ICRP Conversion Coefficients

Since DXT-RAD measured organ-absorbed dose results were compared to MCNP calculated organ-absorbed dose to validate the MCNP model, verification of ICRP conversion coefficients is accomplished by comparing the results of DXT-RAD measured organ-absorbed dose to Panasonic TLD-derived organ-absorbed dose. Tables 6 and 7 in section IV.2 provide the results of comparing the DXT-RAD measured organ-absorbed doses with the Panasonic TLD-derived organ-absorbed doses. The Panasonic TLDs provide results in terms of effective dose for the whole body (called the $H_p(10)$ by ICRP) and, since effective dose and organ-absorbed dose are not the same dosimetry concepts, one must link the two quantities together to demonstrate a relationship. The quantities are linked by converting effective dose into absorbed dose and comparing those derived values to measured results.

V.3.a Description of Panasonic TLD-Derived Organ-Absorbed Dose Results

The Panasonic TLD-derived organ absorbed dose results presented in Tables 6 and 7 were derived from the conversion coefficients found in Table A.24 of ICRP Report No. 74 (1996) and the organ specific tables for geometry corrections found in Appendix A

to ICRP Report No. 74 (1996). It is recognized that Table A.24 of ICRP Report No. 74 (1996) provides these coefficients based upon an ICRU slab and angular dependence factors, but since the TLDs were calibrated on an ICRU slab, this table serves as a suitable surrogate to provide this conversion. The conversion was based on the AP position TLD from monitoring period number one. One of the reasons for using this TLD is that radiation workers are trained to wear TLDs in the AP location unless otherwise instructed and first responders are similarly trained. Another reason for selecting this TLD is that the AP TLD from monitoring period number two measured marginally higher values due to the residual ^{99m}Tc from the previous monitoring period.

Once the first conversion is completed, effective dose is converted to free-in-air kerma, K_a. An additional conversion must be performed to transform K_a into absorbed dose (D_T), through the use of organ-specific and geometry-specific tabulated data in ICRP (1996) Appendix A. This final conversion requires knowledge of both the energy of the incident photon and the geometry of the source. In this case, the ROT geometry was used as a surrogate for the IS geometry. While not precisely the same geometry, the ROT is assumed to be acceptable for use because it is similar to the IS geometry and no other suitable analogue exists.

The final conversion was to correct for the absence of the arm on the phantom. It is recognized that the organs would have received a smaller magnitude of absorbed dose if the phantom possessed arms, but at present this cannot be quantitatively ascertained without additional experiments with a phantom that has arms. To make this correction, a reduction ratio between the RLAT TLD for monitoring period number one and the AP TLD for monitoring period number one was developed by dividing the value of the AP TLD by the value of the RLAT TLD. This reduction ratio was 1.72 and, thus, all organ absorbed

dose results from Table 5 were divided by this factor and results recorded in Tables 6 and 7.

There are two principle reasons why the TLDs from monitoring period number one were used to develop the reduction ratio. First, as stated previously, the results from monitoring period number two were slightly higher due the presence of residual ^{99m}Tc from the previous day. The other reason for excluding the RLAT TLD and including the AP TLD is based on work discussed in ICRP (1996) where the AP position generally receives the highest effective doses. There is, of course, an exception to this where the PA position can receive a higher effective dose. This is because the equivalent dose to the spine is somewhat higher since this organ lies close to the surface of the skin and shielding from the body is minimized, but that is of little significance here.

V.3.b Comparison of DXT-RAD Results to Panasonic TLD Results

A review of Figure 16 and Figure 17 indicate relatively good agreement between DXT-RAD measured organ-absorbed doses and Panasonic TLD-derived organ-absorbed doses. There is a very small disparity among three of the seven organs examined, however. The three disparate organs are the small intestine (SI), colon (includes ascending and transverse), and gall bladder. Specifically, the lower end of the margins of error for the DXT-RAD measured organ-absorbed doses (corrected for the missing arms) do not compare favorably with the higher end margins of error for the Panasonic TLD-derived organ-absorbed doses. This result is not very surprising considering that the phantom used is completely tissue equivalent and has a homogenous density. As defined in the MCNP model, the organs modeled had different densities and thus would estimate different energy depositions, so a single conversion from the AP TLD would contain some inherent error in estimating the true value of organ-absorbed dose. Moreover, the precise

location of these organs is somewhat difficult to identify since the phantom used did not possess specific internal organs. What is worthy to note is that despite these difficulties, use of ICRP (1996) conversion coefficients provided reasonable estimates of organ absorbed doses in the IS and ROT geometry as long as energy and angular dependence were taken into account. Therefore, the ICRP Report No. 74 (1996) conversion coefficients are verified because relatively good agreement exists between DXT-RAD measured organ-absorbed doses and Panasonic TLD-derived organ-absorbed doses.

V.4 Discussion of Full Circle Organ-Absorbed Dose Results

A review of Figure 18 indicates that most organ-absorbed dose results compare favorably with the simulated TLD-derived organ-absorbed doses. There is a very small disparity among three of the fourteen organs examined. The three disparate organs are the bladder, small intestine (SI), and colon (includes ascending, descending, and transverse). Specifically, the lower end of the margins of error for the MCNP-calculated organ-absorbed doses do not compare favorably with the higher end margins of error for the simulated TLD-derived organ-absorbed dose. This result is not very surprising considering that the phantom used is completely tissue equivalent and has a homogenous density. Moreover, the precise location of these organs is somewhat difficult to identify since the phantom used did not possess specific internal organs. Additionally, since the AP TLD was simulated in this scenario, errors in modeling the precise TLD crystal will generate some expected error. What is worthy to note is that despite these difficulties, the use of ICRP (1996) conversion coefficients provided reasonable estimates of organ-absorbed doses in the IS and ROT geometry as long as energy and angular dependence were taken into account.

V.5 Comparison of Panasonic TLD Results to Victoreen 450P Values

Next in comparison is the relationship of Table 5 Panasonic TLD results to the integrated dose recorded by the Victoreen Model 450P in Tables 9 and 10. The Victoreen 450P ionization chamber was oriented between the chest and waist level and simulated to be held by the right hand. The placement of the Victoreen 450P in this location ensured that representative doses and dose rates were recorded consistently. As a basis of comparison, the RLAT TLD from each monitoring period was examined. The RLAT TLD was very close in proximity to the Victoreen 450P so a comparison to these readings is reasonable. The result of the examination is that the RLAT TLD from monitoring period number one was 1.12 $\pm$ 0.11 mSv and the Victoreen 450P was 1.17 $\pm$ 0.23 mSv. The RLAT TLD from monitoring period two was 1.23 $\pm$ 0.12 mSv and the Victoreen 450P was 1.30 $\pm$ 0.26 mSv. These results indicate that placement of the Victoreen 450P was appropriate and that the instrument values were close in agreement to TLD measured values. In a practical sense, the AP TLD will most likely be the TLD worn by a first responder and so one must compare the Victoreen 450P value to the AP TLD.

The AP TLD measured 0.65 $\pm$ 0.07 mSv in monitoring period number one and 0.73 $\pm$ 0.07 mSv in monitoring period number two. Comparison of the AP TLD results with the Victoreen 450P values (1.30 $\pm$ 0.26 mSv) indicate that the Victoreen 450P provides an overestimate of effective dose by about a factor of two. This also indicates that the Victoreen 450P might possibly serve as a very good real-time indicator of effective dose and organ-absorbed dose if the appropriate corrections for energy and angular dependence and use of appropriate conversion coefficients for energy and geometry are made. Additional experimentation is needed before this could be justified, however. One will note that the value of 0.73 $\pm$ 0.07 mSv is somewhat higher than expected when

compared to the AP TLD value from monitoring period number one and the corresponding RLAT TLD. It is believed that the Victoreen 450P may have been inadvertently brushed against when exchanging dosimeters between experiments. Even slight movement of the Victoreen instrument can change the solid angle of incidence of the radiation field significantly since the AP TLD is a small "target." Brushing against the Victoreen instrument appears to have either shielded the monitoring period number one AP TLD or made more visible the monitoring period number two AP TLD. Additional experimentation is needed to verify this hypothesis.

V.6 Significance to First Responders

In general, radiation workers and first responders are trained to wear TLDs on the chest or waist, which is in the AP position. Also, it is important to note that first responders become *de facto* radiation workers when responding to an incident involving radioactive material. Consequently, first responders are permitted to receive the same amount of annual internal and external radiation exposure as other radiation workers in industry. This is an important consideration when one observes the results of comparing the effective dose of the TLD to the measured values of organ-absorbed dose. Also for radiation protection purposes the organ-absorbed dose is assumed to be equal to the effective dose measured by the TLD.

Realizing that the value of the AP TLD in monitoring period number one from Table 6 in section IV.2 is 0.65 ± 0.07 mSv, the mean value of organ-absorbed dose in Table 7 is 0.46 ± 0.09 mSv, and the Victoreen 450P effective dose value is 1.17 ± 0.26 mSv, one can reason that the AP TLD and Victoreen 450P could represent an overestimate of organ-absorbed dose. For example, the AP TLD, on average, over-estimates the organ-absorbed dose by a factor of about 1.4 (range of over-response for all measured organs is 1.2 to 1.7)

and the Victoreen 450P over-estimates organ-absorbed dose by about a factor of 2.5 (range of over-response for all measured organs is 2.2 to 3). Additionally, the Victoreen 450P over-estimates effective dose by a factor of 1.8 (approximately 2). This statement, of course, is under the assumption that ^{99m}Tc is the radioactive material to which the first responder is exposed and is in the ROT geometry. Nevertheless, if a first responder had a Victoreen 450P in hand, was responding to an RDD event, and the suspected radionuclide was a gamma emitter, the responder could perform a self-estimate of organ-absorbed dose and effective dose in the field by dividing the Victoreen 450P integrated reading by a factor of three and two, respectively.

V.7 Importance to the Incident Commander

This notion is important to the IC because of the decisions needed to determine placement of hazard boundaries. Musolino and Harper (2006) propose that for a very large source with sophisticated engineering, one could observe a groundshine dose of about 1 Gy during a 24-hour exposure period atabout 300 meters from the epicenter of the event. In addition, Musolino and Harper (2006) propose that the level at which emergency personnel can work unrestricted for five hours is equal to 50 mSv at a distance of about 100 meters from an intermediate sized source, and up to about 600 meters from a very large source with sophisticated engineering. In this regard, an IC will decide where to place such boundaries based upon hand-held instrument readings such as the Victoreen 450P ionization chamber. If the Victoreen 450P was used, then the IC could increase the boundary limitations by a factor of two, as read by the Victoreen 450P since this virtual increase would only result in a first responder receiving the actual expected effective dose and associated risk to the responder would not increase.

In addition to the proposed placement of hazard boundaries above, Musolino and

Harper (2006) propose other boundary conditions for evacuation, sheltering in place, and initiating protective actions as described in section I of this investigation. These recommendations are based upon a 50-year committed dose, and in the case of external exposure, this type of decision would be made by the IC based upon hand-held instrument readings such as the Victoreen 450P. Again, we see the over-estimate by the Victoreen for organ dose, where the over-estimate is about a factor of three. Therefore, the IC could increase action levels by a factor of three, as read by the Victoreen 450P since this virtual increase would only result in a first responder receiving the actual expected organ dose and associated risk to the responder would not increase.

VI. CONCLUSIONS

Several conclusions can be drawn from this investigation. The selection of $Na^{99m}TcO_4$ served as a good initial source of radioactive material to conduct this investigation. The material was easy to obtain, measure and dispose. It also had a short half-life so that larger quantities could be used without concern for disposal costs. Additionally, the liquid form of the $Na^{99m}TcO_4$ facilitated dispersal of the material to ensure uniform distribution of the source.

Another conclusion is that the semi-circular source used to define the IS geometry indicates that the ICRP (1996) ROT geometry is a suitable surrogate for the IS geometry and is a suitable approximation to that of a radiological dispersal device. Therefore, the first objective is satisfied. In addition, the Rando® phantom, Panasonic TLDs, DXT-RAD dosimeters, and Victoreen 450P instruments are commonly found at many facilities. These devices are used to monitor individuals and provide radiological protection and, thus, provide a reasonable means to conduct additional experiments with a high degree of repeatability. Therefore, this provides an inexpensive means to conduct future experiments should funding and other resources become available.

The additional modeling conducted with a three meter radius full circle source confirms that the investigational IS geometry is a suitable surrogate for the ROT geometry, MCNP modeling of the human body is accomplished reasonably well, and photon transport in air and tissue using MCNP is effective. The investigation concludes that MCNP modeling for different energies of photons and geometries of exposure will be effective and reliable. For more accurate assessments, however, a phantom that contains specific organs with related tissue densities is recommended, or even a more homogenous

phantom model.

This investigation measured organ absorbed doses inside a tissue equivalent phantom, compared these values to the effective doses measured using Panasonic TLDs and MCNP modeled results and found that most measured values compared favorably with the organ-absorbed dose-derived values from the Panasonic TLD and the MCNP model. Therefore, the MCNP model was assumed to be validated and the second, third, and fifth objectives are satisfied. In addition, the Victoreen 450P values of integrated dose compared well with the Panasonic RLAT TLD and, thus, ensured that placement of the Victoreen 450P was justified. This also demonstrated that the Victoreen 450P could potentially serve as an estimator of real-time effective dose and organ absorbed dose provided that energy and angular dependence could be taken into account. Therefore, the fourth objective is satisfied.

In conclusion, the data presented in this investigation indicate that the MCNP model developed provided a reasonable approximation to measured results of the simulated RDD in an IS geometry with $Na^{99m}TcO_4$ as the source of radioactive material. Additional investigation is needed, however, with other sources of radioactive material such as ^{137}Cs, ^{60}Co, ^{192}Ir, and $^{90}Sr/^{90}Y$. Along with other sources of radioactive material is the need to use an organ-specific phantom that has articulated joints at the shoulders, elbows, hips, and knees because a more realistic first responder geometry is for a person to be in the crouched position rather than standing vertically. Such a phantom exists at the Pacific Northwest National Laboratory in Richland, Washington, but availability of funding for its use and the demands on its use by the existing facility present procurement difficulties. Using this type of phantom provides a means to model and measure many different exposure geometries for each radionuclide in the investigation and, thus, provide a more

comprehensive database of doses received from an RDD. Additional research needs are in the areas of particle tracking to determine dose to a specified target. Of great value would be to obtain the energy and angle of the incident radiation with the dosimetric region of interest. By knowing the spectrum of energies and angles that impinge on internal organs, one may be able to make the appropriate corrections more precisely. This will enable any interested party to better determine the non-uniform distribution of energy deposited in organs versus depth.

REFERENCES

American Cancer Society, Probability of developing invasive cancers over selected age intervals by sex, US, 2000 to 2002, Surveillance Research, Statistical Research and Applications Branch, Bethesda, Md: National Cancer Institute; 2005.

Attix, F. H. Further consideration of the track-interaction model for thermoluminescence in LiF (TLD-100). Journal of Applied Physics, 46(81), 86-135; 1975.

Attix, F.H. Introduction to radiological physics and radiation dosimetry. New York: Wiley-Interscience; 1986.

Briesmeister, J. F. Ed. MCNP™- a general Monte Carlo N-particle transport code Version 4C. Los Alamos National Laboratory, LA-13709-M; 2000.

Brown, W. H. Organic chemistry. Orlando, Fl: Harcourt Brace & Company; 1995.

Cember, H. Introduction to health physics. Third Edition. New York: McGraw Hill; 1996.

Department of Homeland Security (DHS). *Protective action guides for radiological dispersal device and improvised nuclear device incidents.* Washington, DC: Department of Homeland Security; 2006.

Environmental Protection Agency (EPA). Manual of protective action guides and protective actions for nuclear incidents. Washington, DC. Environmental Protection Agency; 1992.

Federal Bureau of Investigation (FBI). Weapons of mass destruction incident contingency plan. Washington, DC. Federal Bureau of Investigation; 1998.

International Commission on Radiological Protection (ICRP). Report of the task group of Reference Man. ICRP Publication 23. Oxford: Pergamon Press; 1975.

International Commission on Radiological Protection (ICRP). Recommendations of the International Commission on Radiological Protection, ICRP Publication 60. Annals of the ICRP, Oxford: Pergamon Press; 1991.

International Commission on Radiological Protection (ICRP). Conversion coefficients for use in radiological protection against external radiation. ICRP Publication 74. Annals of the ICRP. Vol 26 (3/4), Oxford: Pergamon Press, 1996.

International Commission on Radiation Units and Measurements (ICRU). Determination of dose equivalents resulting from external radiation sources. ICRU Report 39. Bethesda, Md: International Commission on Radiation Units and Measurements; 1985.

International Commission on Radiation Units and Measurements (ICRU). Determination of

dose equivalents from external radiation sources – part 2. ICRU Report 43. Bethesda, Md: International Commission on Radiation Units and Measurements; 1988.

International Commission on Radiation Units and Measurements (ICRU). Measurements of dose equivalents from external photon and electron radiations. ICRU Report 47. Bethesda, Md: International Commission on Radiation Units and Measurements; 1992.

International Commission on Radiation Units and Measurements (ICRU). Quantities and units in radiation protection dosimetry. ICRU Report 51. Bethesda, Md: International Commission on Radiation Units and Measurements; 1993.

Lushbaugh, C.C., Ricks, R.C. Some cytokinetic and histopathologic considerations of irradiated male and female gonadal tissues. In: J.M. Veath, and S. Karger, eds. Frontiers of Radiation Therapy and Oncology. New York, NY: Wiley and Sons; 1972: Vol. 6, 228-248.

Musolino, Stephen V., Harper, Frederick T. Emergency response guidance for the first 48 hours after the outdoor detonation of an explosive radiological dispersal device. Health Physics, 90(4): 163-166, April 2006.

National Council on Radiation Protection and Measurements (NCRP). A handbook of radioactivity measurements procedures: with nuclear data for some biologically important radionuclides. Recommendations of the National Council on Radiation Protection and Measurements. NCRP Report 58. Washington, DC: National Council on Radiation Protection and Measurements; 1978.

National Council on Radiation Protection and Measurements (NCRP). Management of terrorist events involving radioactive material; Recommendations of the National Council on Radiation Protection and Measurements. NCRP Report 138. Washington, DC: National Council on Radiation Protection and Measurements; 2001.

National Response Plan (NRP) Department of Homeland Security. National response plan. Washington, DC: Department of Homeland Security; 2004.

Nuclides and Isotopes. Knolls Atomic Power Laboratory. Chart of the Nuclides. Schenectedy, NY: Lockheed Martin Company; 2002.

Pederson, K., Andersen, T., Rodal, J., Olsen, D., Sensitivity and stability of LiF thermoluminescent dosimeters. Medical Dosimetry, 20(4), 263-267; 1995.

Shikata, E., Iguchi, A. Production of ^{99}Mo and its application in nuclear medicine. Journal of Radioanalytical Nuclear Chemistry, Articles 102 (2), 533–550; 1986.

Tuli, J.K., Reed, G., Singh, B., Nuclear data sheets for ^{99m}Tc. Nuclear Data Sheets. 93(1), 86-87; May 2001.

U.S. Nuclear Regulatory Commission (NRC), Title 10, Code of Federal Regulations, Part 20, Standards for Protection Against Radiation. Washington, DC: Nuclear Regulatory Commission; 1991.

APPENDIX A

A.1 Monitoring Period One DXT-RAD Results

Table A1: Monitoring period one DXT-RAD results.

Slice 31 0 cm								
Slice Number/ DXT Serial Number	photon /beta (mrad)	Slice Number/ DXT Serial Number	photon/ beta (mrad)	Slice Number/ DXT Serial Number	photon /beta (mrad)	Slice Number	Slice Number / DXT Serial Number	photon /beta (mrad)
A1/9923	132.1/ 151	A2		A3/8628	79.4/90	A4		
B1		B2		B3		B4		
C1/7439	125.9/ 144	C2		C3/8098	78.1/88	C4		
D1		D2		D3		D4		
E1/10339	115.3/ 132	E2		E3/7387	77/87	E4		
F1		F2		F3/8071	90.8/10 3	F4	F5/8254	79.1/9 0
Slice 30 2.5 cm								
A1/8847	119/13 6	A2		A3/7968	77.5/88	A4		
B1		B2		B3		B4		
C1/7711	113.1/ 129	C2		C3/8016	75.7/86	C4		
D1		D2		D3		D4		
E1/8207	113.5/ 129	E2		E3/8037	79.8/90	E4		
F1		F2		F3/8065	92.2/10 5	F4	F5/8078	75.4/8 5
Slice 29 5 cm								
A1/7386	114.9/ 131	A2		A3/10350	83.5/95	A4		

B1		B2		B3		B4		
C1/7937	115.3/132	C2		C3/8492	73.7/83	C4		
D1		D2		D3		D4		
E1/8693	122.3/140	E2		E3/8119	81.8/93	E4		
F1		F2		F3/8684	89.8/102	F4	F5/8217	75.9/86
Slice 28 7.5 cm								
Slice Number/ DXT Serial Number	photon /beta (mrad)	Slice Number/ DXT Serial Number	photon/ beta (mrad)	Slice Number/ DXT Serial Number	photon/ beta (mrad)	Slice Number /DXT Serial Number	photon/ beta (mrad)	
A1/8220	125.9/144	A2		A3/8036	78.5/89	A4		
B1/8435	109.2/124	B2		B3/7475	74.7/84	B4		
C1/8467	116.2/133	C2		C3/7835	74.8/85	C4		
D1		D2/8018	91.9/104	D3		D4/8460	70.9/80	
E1		E2		E3		E4		
F1		F2		F3		F4		
Slice 27 10 cm								
A1		A2/8601	102.3/116	A3/8054	84.9/96	A4		
B1/8918	109.1/124	B2		B3/8052	79.5/90	B4		
C1/8213	106.2/121	C2		C3/7970	73.7/83	C4		
D1		D2/9780	84.6/96	D3		D4/9818	71/80	
E1		E2		E3		E4		
F1		F2		F3		F4		
Slice 26 12.5 cm								
A1		A2/8612	104.4/119	A3/8512	8702/99	A4		
B1/8023	121.2/138	B2		B3/8133	76/86	B4		
C1/8397	118.3/135	C2		C3/8867	79.7/90	C4		
D1		D2/9998	91.8/10	D3		D4/880	69.3/78	

			4			0		
E1		E2		E3		E4		
F1		F2		F3		F4		
Slice 25 15 cm								
Slice Number/ DXT Serial Number	photon /beta (mrad)	Slice Number/ DXT Serial Number	photon/ beta (mrad)	Slice Number/ DXT Serial Number	photon/ beta (mrad)	Slice Number /DXT Serial Number	photon/ beta (mrad)	
A1		A2		A3		A4		
B1		B2		B3		B4		
C1/10853	130.9/ 150	C2/8297	93.1/10 6	C3/7506	83.2/94	C4/847 1	64.6/73	
D1/8682	127.2/ 145	D2/8657	90.5/10 3	D3/8672	77.1/87	D4/850 2	69.7/79	
E1		E2		E3		E4		
F1		F2		F3		F4		
Slice 24 17.5 cm								
A1		A2		A3		A4		
B1		B2		B3		B4		
C1/8004	122.6/ 140	C2/8907	96.2/10 9	C3/8425	78/88	C4/869 6	67.4/76	
D1/8222	114.9/ 131	D2/8088	97.2/11 1	D3/9536	80.9/92	D4/744 2	69.1/78	
E1		E2		E3		E4		
F1		F2		F3		F4		
Slice 23 20 cm								
A1		A2		A3		A4		
B1		B2		B3		B4		
C1/8163	124.5/ 143	C2/8294	91.6/10 4	C3/8227	76.8/87	C4/826 6	66.2/75	
D1/8968	118.4/ 135	D2/8836	98.7/11 2	D3/8080	80/91	D4/897 1	68.2/77	
E1		E2		E3		E4		
F1		F2		F3		F4		
Slice 22 22.5 cm								

A1		A2		A3		A4		
B1		B2		B3		B4		
C1/9977	120/137	C2/8732	91.7/104	C3/7219	76.4/86	C4/8636	67.8/76	
D1/8014	116.3/133	D2/8153	90.6/103	D3/9886	76.6/87	D4/7548	66.2/75	
E1		E2		E3		E4		
F1		F2		F3		F4		
Slice 21 25 cm								
Slice Number/ DXT Serial Number	photon /beta (mrad)	Slice Number/ DXT Serial Number	photon/ beta (mrad)	Slice Number/ DXT Serial Number	photon/ beta (mrad)	Slice Number /DXT Serial Number	photon/ beta (mrad)	
A1		A2		A3		A4		
B1		B2		B3		B4		
C1/7008	105.6/120	C2/9684	92.2/105	C3/9148	81.8/93	C4/8649	63.5/71	
D1/7231	105.4/120	D2/7686	92.6/105	D3/8501	77.8/89	D4/7555	65.2/73	
E1		E2		E3		E4		
F1		F2		F3		F4		
Slice 20 27.5 cm								
A1		A2		A3		A4		
B1		B2		B3		B4		
C1		C2/8451	93.8/107	C3/8085	74.8/85	C4/8599	62.2/70	
D1/8008	103.8/118	D2/8913	89.7/102	D3/8715	72.2/82	D4/8691	61.9/70	
E1		E2		E3/9448	76.7/87	E4		
F1		F2		F3		F4		
Slice 19 30 cm								
A1		A2		A3		A4		
B1		B2		B3		B4		
C1		C2/7019	84.2/95	C3/8510	76.7/87	C4/8164	68.8/78	
D1/7157	100.2/114	D2/8003	92.3/105	D3/8387	79/89	D4/7433	66.8/75	
E1		E2		E3/8024	71.6/81	E4		
F1		F2		F3		F4		

Slice 18 32.5 cm								
A1		A2		A3		A4		
B1		B2		B3		B4		
C1		C2/8121	93.6/106	C3/7612	76.5/87	C4		
D1/8063	96.5/110	D2/8518	90/102	D3/7082	79.1/90	D4/8811	70.2/79	
E1		E2/8652	96.8/110	E3/8134	85.3/97	E4		
F1		F2		F3		F4		
Slice 17 35 cm								
Slice Number/ DXT Serial Number	photon /beta (mrad)	Slice Number/ DXT Serial Number	photon/ beta (mrad)	Slice Number/ DXT Serial Number	photon/ beta (mrad)	Slice Number /DXT Serial Number	photon/ beta (mrad)	
A1		A2		A3		A4		
B1		B2		B3		B4		
C1		C2/7800	86.2/98	C3/7382	80.8/92	C4		
D1/8448	93.3/106	D2/10097	87.9/100	D3/7494	81.6/92	D4/8264	73/82	
E1		E2/8486	87.6/99	E3/8386	85.5/97	E4		
F1		F2		F3		F4		
Slice 16 37.5 cm								
A1		A2		A3		A4		
B1		B2		B3		B4		
C1		C2/8625	80.1/91	C3/8371	73.1/83	C4		
D1/7293	92.8/105	D2/8556	82.7/94	D3/9618	82.3/93	D4/8705	78.3/89	
E1		E2/7698	83.3/94	E3/8587	79.8/90	E4		
F1		F2		F3		F4		

A.2 Monitoring Period Two DXT-RAD Results

Table A2: Monitoring period two DXT-RAD results.

Slice 31 0 cm								
Slice Number/ DXT Serial Number	photon/beta (mrad)	Slice Number/ DXT Serial Number	photon/beta (mrad)	Slice Number/ DXT Serial Number	photon/beta (mrad)	Slice Number	Slice Number/ DXT Serial Number	photon/ beta (mrad)
A1/8177	123.2/141	A2		A3/8419	90/102	A4		
B1		B2		B3		B4		
C1/8242	110.8/126	C2		C3/8438	78.3/89	C4		
D1		D2		D3		D4		
E1/8034	127.9/146	E2		E3/10501	90.8/103	E4		
F1		F2		F3/8846	89.6/102	F4	F5/7704	79.5/90
Slice 30 2.5 cm								
A1/8021	127.9/146	A2		A3/7553	75.7/86	A4		
B1		B2		B3		B4		
C1/9744	107.9/123	C2		C3/8073	77/87	C4		
D1		D2		D3		D4		
E1/8384	125.9/144	E2		E3/8545	92.1/105	E4		
F1		F2		F3/8404	102.3/116	F4	F5/8639	71.6/81
Slice 29 5 cm								
A1/9957	134.4/154	A2		A3/8698	86.3/98	A4		
B1		B2		B3		B4		
C1/8200	114.1/130	C2		C3/8273	83.3/94	C4		
D1		D2		D3		D4		

E1/8595	116/132	E2		E3/8945	84.8/96	E4		
F1		F2		F3/8779	100.8/115	F4	F5/7882	72.3/82
Slice 28 7.5 cm								
Slice Number/ DXT Serial Number	photon/beta (mrad)	Slice Number/ DXT Serial Number	photon/beta (mrad)	Slice Number/ DXT Serial Number	photon/beta (mrad)	Slice Number/ DXT Serial Number	photon/ beta (mrad)	
A1/8360	120.8/138	A2		A3/8346	86.8/98	A4		
B1/8327	127.2/145	B2		B3/9900	78.8/89	B4		
C1/8865	115.2/131	C2		C3/8316	77.1/87	C4		
D1		D2/7495	103.1/117	D3		D4/8525	68.4/77	
E1		E2		E3		E4		
F1		F2		F3		F4	F5	
Slice 27 10 cm								
A1		A2/8374	103.2/117	A3/8567	82.7/94	A4		
B1/8103	123.7/141	B2		B3/7229	79/89	B4		
C1/7874	114.5/131	C2		C3/10255	80.4/91	C4		
D1		D2/7525	101.7/116	D3		D4/9156	71/80	
E1		E2		E3		E4		
F1		F2		F3		F4		
Slice 26 12.5 cm								
A1		A2/7931	97.6/111	A3/8051	88.2/100	A4		
B1/8410	136.4/156	B2		B3/7252	79.8/90	B4		
C1/8605	120.2/137	C2		C3/8611	80.7/91	C4		
D1		D2/9932	96.9/110	D3		D4/7909	68.9/78	
E1		E2		E3		E4		

F1		F2		F3		F4		
Slice 25 15 cm								
Slice Number/ DXT Serial Number	photon/beta (mrad)	Slice Number/ DXT Serial Number	photon/beta (mrad)	Slice Number/ DXT Serial Number	photon/beta (mrad)	Slice Number/ DXT Serial Number	photon/ beta (mrad)	
A1		A2		A3		A4		
B1		B2		B3		B4		
C1/8950	132/151	C2/9278	98.1/112	C3/8381	80/91	C4/8815	68.4/77	
D1/9713	129.6/148	D2/8789	95.7/109	D3/7727	84.7/96	D4/8841	65.7/74	
E1		E2		E3		E4		
F1		F2		F3		F4		
Slice 24 17.5 cm								
A1		A2		A3		A4		
B1		B2		B3		B4		
C1/8146	129/147	C2/9897	103.8/118	C3/8020	80.8/92	C4/8417	65.9/74	
D1/8218	122.8/140	D2/8047	100.1/114	D3/8955	82.9/94	D4/8897	68.7/77	
E1		E2		E3		E4		
F1		F2		F3		F4		
Slice 23 20 cm								
A1		A2		A3		A4		
B1		B2		B3		B4		
C1/8798	125.9/144	C2/8711	100.4/114	C3/8788	79.1/90	C4/10046	68.3/77	
D1/8109	126/144	D2/7597	100.9/115	D3/8819	82.5/93	D4/8880	72.8/82	
E1		E2		E3		E4		
F1		F2		F3		F4		
Slice 22 22.5 cm								

A1		A2		A3		A4		
B1		B2		B3		B4		
C1/8289	119.6/137	C2/7867	98.1/112	C3/8000	74.8/85	C4/8369	67.5/76	
D1/7549	114.8/131	D2/7444	96.7/110	D3/8726	78.3/89	D4/8916	72.2/82	
E1		E2		E3		E4		
F1		F2		F3		F4		
Slice 21 25 cm								
Slice Number/ DXT Serial Number	photon/beta (mrad)	Slice Number/ DXT Serial Number	photon/beta (mrad)	Slice Number/ DXT Serial Number	photon/beta (mrad)	Slice Number/ DXT Serial Number	photon/ beta (mrad)	
A1		A2		A3		A4		
B1		B2		B3		B4		
C1/7262	110.1/125	C2/9208	95.1/108	C3/8333	75.1/85	C4/7216	68/77	
D1/8593	109.7/125	D2/8637	91.4/104	D3/8754	82.8/94	D4/8891	65/73	
E1		E2		E3		E4		
F1		F2		F3		F4		
Slice 20 27.5 cm								
A1		A2		A3		A4		
B1		B2		B3		B4		
C1		C2/8256	100.2/114	C3/8671	80.3/91	C4/8723	63.1/71	
D1/9120	114.6/131	D2/8002	92.8/105	D3/8412	80.2/91	D4/8087	66.7/75	
E1		E2		E3/7755	79.9/90	E4		
F1		F2		F3		F4		
Slice 19 30 cm								
A1		A2		A3		A4		
B1		B2		B3		B4		
C1		C2/9225	93.2/106	C3/8785	81.6/92	C4/8889	69.2/78	
D1/8782	101.5/116	D2/8372	96.7/110	D3/7441	75.7/86	D4/7611	62.9/71	
E1		E2		E3/8544	71.5/81	E4		

F1		F2		F3		F4		
Slice 18 32.5 cm								
Slice Number/ DXT Serial Number	photon/beta (mrad)	Slice Number/ DXT Serial Number	photon/beta (mrad)	Slice Number/ DXT Serial Number	photon/beta (mrad)	Slice Number/ DXT Serial Number	photon/ beta (mrad)	
A1		A2		A3		A4		
B1		B2		B3		B4		
C1		C2/8366	94.2/107	C3/8928	80.2/91	C4		
D1/9396	97.8/111	D2/7070	94.5/107	D3/10009	84.4/96	D4/8015	70.2/79	
E1		E2/7175	96.9/110	E3/8199	83.9/95	E4		
F1		F2		F3		F4		
Slice 17 35 cm								
A1		A2		A3		A4		
B1		B2		B3		B4		
C1		C2/8365	98.8/112	C3/8215	84.6/96	C4		
D1/7670	99.8/114	D2/7523	97.5/112	D3/8608	86/98	D4/8099	76.2/86	
E1		E2/8797	97.3/111	E3/7545	85.1/96	E4		
F1		F2		F3		F4		
Slice 16 37.5 cm								
A1		A2		A3		A4		
B1		B2		B3		B4		
C1		C2/7881	84/95	C3/8233	82.7/94	C4		
D1/9808	103.7/118	D2/8009	90.3/103	D3/8427	86.2/98	D4/8026	78.6/89	
E1		E2/8848	91.4/104	E3/8938	95.8/109	E4		
F1		F2		F3		F4		

APPENDIX B

B.1 Monitoring Period One Radiological Survey Parameters

Table B1: Radiological monitoring parameters for monitoring period one.

Radiological Monitoring Parameters		
Time	Dose Rate (mSv h^{-1})	Integrated Dose (mSv)
0	0.073 ± 0.015	0
4	0.05 ± 0.01	0.28 ± 0.06
8	0.085 ± 0.017	0.6 ± 0.12
12	0.055 ± 0.01	0.85 ± 0.17
24	0.015 ± 0.003	1.17 ± 0.23

B.2 Monitoring Period Two Radiological Survey Parameters

Table B1: Radiological monitoring parameters for monitoring period two.

Radiological Monitoring Parameters		
Time	Dose Rate ($mSv\ h^{-1}$)	Integrated Dose (mSv)
0	0.08 ± 0.016	0
4	0.052 ± 0.010	0.32 ± 0.06
8	0.095 ± 0.019	0.68 ± 0.14
12	0.062 ± 0.012	0.95 ± 0.19
24	0.017 ± 0.003	1.3 ± 0.26

APPENDIX C

C.1 Monitoring Period One Organ-Specific Results.

Table C1: The measured and calculated absorbed dose results for the small intestine

Slice/Position	Measured Results[1] (mSv)	Calculated Results[3] (mSv)	Percentage Error (%)
31/A1	1.32 ± 0.132	1.15 ± 0.05	14.8
31/C1	1.26 ± 0.126	1.08 ± 0.05	16.7
31/E3	0.77 ± 0.077	0.62 ± 0.09	24.2
31/F3	0.91 ± 0.091	0.74 ± 0.07	23.0
31/F5	0.79 ± 0.079	0.59 ± 0.09	33.9
30/A1	1.19 ± 0.119	1.02 ± 0.05	16.7
30/C1	1.13 ± 0.113	0.98 ± 0.06	15.3
30/E3	0.8 ± 0.08	0.65 ± 0.05	23.1
Average	**1.02 ± 0.24[2]**	**0.85 ± 0.06[2]**	**20.9**

1) Results are rounded up to the nearest tenth and slice/position error is calculated as ±10% error based on phone communications with Michael Klueber at the US Air Force Radiation Dosimetry Branch.
2) Overall system error is calculated as the square root of the sum of the squares of the standard deviation and measurement error, per guidance in NCRP Report 58.
3) Error in these calculated results are expressed as relative error, where MCNP defines relative error, $R = \sigma / \bar{x}$, where σ is the standard deviation of the mean and $\bar{x}$ is the mean,

Table C2: The measured and calculated absorbed dose results for the kidney.

Slice/Position	Measured Results[1] (mSv)	Calculated Results[3] (mSv)	Percentage Error (%)
31/A3	0.79 ± 0.079	0.65 ± 0.05	21.5
31/C3	0.78 ± 0.078	0.65 ± 0.06	20.0
30/A3	0.78 ± 0.078	0.63 ± 0.06	23.8
30/C3	0.76 ± 0.076	0.61 ± 0.05	24.6
29/A3	0.84 ± 0.084	0.72 ± 0.04	16.7
28/A3	0.79 ± 0.079	0.68 ± 0.05	16.2
28/B3	0.75 ± 0.075	0.65 ± 0.06	15.4
27/A3	0.85 ± 0.085	0.73 ± 0.04	16.4
27/B3	0.8 ± 0.08	0.69 ± 0.07	15.9
Average	**0.79 ± 0.10[2]**	**0.67 ± 0.05[2]**	**18.9**

1) Results are rounded up to the nearest tenth and slice/position error is calculated as ±10% error based on phone communications with Michael Klueber at the US Air Force Radiation Dosimetry Branch.
2) Overall system error is calculated as the square root of the sum of the squares of the standard deviation and measurement error, per guidance in NCRP Report 58.
3) Error in these calculated results are expressed as relative error, where MCNP defines relative error, $R = \sigma / \bar{x}$, where σ is the standard deviation of the mean and $\bar{x}$ is the mean.

Table C3: The measured and calculated absorbed dose results for the liver.

Slice/Position	Measured Results[1] (mSv)	Calculated Results[3] (mSv)	Percentage Error (%)
29/A1	1.15 ± 0.115	0.91 ± 0.050	26.4
29/C1	1.15 ± 0.115	0.91 ± 0.049	26.4
29/C3	0.74 ± 0.074	0.55 ± 0.051	34.5
29/E1	1.22 ± 0.122	1.08 ± 0.050	13.0
28/A1	1.26 ± 0.126	1.1 ± 0.054	14.5
28/B1	1.09 ± 0.109	1.02 ± 0.048	6.9
28/C1	1.16 ± 0.116	0.99 ± 0.054	17.2
28/C3	0.75 ± 0.075	0.59 ± 0.063	27.1
27/B1	1.09 ± 0.109	0.87 ± 0.049	25.3
27/C1	1.06 ± 0.106	0.89 ± 0.049	19.1
27/D4	0.71 ± 0.071	0.53 ± 0.088	34.0
26/B1	1.21 ± 0.121	1.1 ± 0.051	10.0
26/C1	1.18 ± 0.118	1.04 ± 0.046	13.5
26/D4	0.69 ± 0.069	0.58 ± 0.09	19.0
25/C1	1.31 ± 0.131	1.16 ± 0.05	12.9
25/C2	0.93 ± 0.093	0.74 ± 0.062	25.7
25/C3	0.83 ± 0.083	0.68 ± 0.058	22.1
25/C4	0.65 ± 0.065	0.54 ± 0.08	20.4
25/D1	1.27 ± 0.127	1.15 ± 0.058	10.4
25/D2	0.91 ± 0.091	0.75 ± 0.061	21.3
25/D3	0.77 ± 0.077	0.62 ± 0.065	24.2
25/D4	0.7 ± 0.07	0.61 ± 0.089	14.8
24/C1	1.23 ± 0.123	1.08 ± 0.050	13.9
24/C2	0.96 ± 0.096	0.81 ± 0.064	18.5
24/C3	0.78 ± 0.078	0.61 ± 0.064	27.9
24/C4	0.67 ± 0.067	0.51 ± 0.073	31.4
24/D1	1.15 ± 0.115	1 ± 0.047	15.0
24/D2	0.97 ± 0.097	0.82 ± 0.051	18.3
24/D3	0.81 ± 0.081	0.68 ± 0.06	19.1
24/D4	0.69 ± 0.069	0.54 ± 0.093	27.8
Average	**0.97 ± 0.24[2]**	**0.82 ± 0.06[2]**	**20.3**

1) Results are rounded up to the nearest tenth and slice/position error is calculated as ±10% error based on phone communications with Michael Klueber at the US Air Force Radiation Dosimetry Branch.
2) Overall system error is calculated as the square root of the sum of the squares of the standard deviation and measurement error, per guidance in NCRP Report 58.
3) Error in these calculated results are expressed as relative error, where MCNP defines relative error, $R = \sigma / \bar{x}$, where σ is the standard deviation of the mean and $\bar{x}$ is the mean.

Table C4: The measured and calculated absorbed dose results for the ascending colon.

Slice/Position	Measured Results[1] (mSv)	Calculated Results[3] (mSv)	Percentage Error (%)
31/E1	1.15 ± 0.12	0.97 ± 0.057	18.6
30/E1	1.14 ± 0.11	0.95 ± 0.050	20.0
29/E3	0.82 ± 0.08	0.67 ± 0.088	22.4
Average	**1.04 ± 0.18[2]**	**0.86 ± 0.07[2]**	**20.3**

1) Results are rounded up to the nearest tenth and slice/position error is calculated as ±10% error based on phone communications with Michael Klueber at the US Air Force Radiation Dosimetry Branch.
2) Overall system error is calculated as the square root of the sum of the squares of the standard deviation and measurement error, per guidance in NCRP Report 58.
3) Error in these calculated results are expressed as relative error, where MCNP defines relative error, $R = \sigma / \bar{x}$, where σ is the standard deviation of the mean and $\bar{x}$ is the mean.

Table C5: The measured and calculated absorbed dose results for the transverse colon.

Slice/Position	Measured Results[1] (mSv)	Calculated Results[3] (mSv)	Percentage Error (%)
30/F3	0.92 ± 0.09	0.75 ± 0.048	22.7
30/F5	0.75 ± 0.08	0.61 ± 0.041	23.0
29/F3	0.9 ± 0.09	0.74 ± 0.047	21.6
29/F5	0.76 ± 0.08	0.62 ± 0.042	22.6
Average	**0.83 ± 0.13[2]**	**0.68 ± 0.04[2]**	**22.5**

1) Results are rounded up to the nearest tenth and slice/position error is calculated as ±10% error based on phone communications with Michael Klueber at the US Air Force Radiation Dosimetry Branch.
2) Overall system error is calculated as the square root of the sum of the squares of the standard deviation and measurement error, per guidance in NCRP Report 58.
3) Error in these calculated results are expressed as relative error, where MCNP defines relative error, $R = \sigma / \bar{x}$, where σ is the standard deviation of the mean and $\bar{x}$ is the mean.

Table C6: The measured and calculated absorbed dose results for the gall bladder.

Slice/Position	Measured Results[1] (mSv)	Calculated Results[3] (mSv)	Percentage Error (%)
28/D2	0.92 ± 0.09	0.75 ± 0.005	22.7
27/D2	0.85 ± 0.09	0.68 ± 0.056	25.0
26/D2	0.92 ± 0.09	0.76 ± 0.005	21.1
Average	**0.90 ± 0.11[2]**	**0.73 ± 0.03[2]**	**22.9**

1) Results are rounded up to the nearest tenth and slice/position error is calculated as ±10% error based on phone communications with Michael Klueber at the US Air Force Radiation Dosimetry Branch.
2) Overall system error is calculated as the square root of the sum of the squares of the standard deviation and measurement error, per guidance in NCRP Report 58.
3) Error in these calculated results are expressed as relative error, where MCNP defines relative error, $R = \sigma / \bar{x}$, where σ is the standard deviation of the mean and $\bar{x}$ is the mean.

Table C7: The measured and calculated absorbed dose results for the pancreas.

Slice/Position	Measured Results[1] (mSv)	Calculated Results[3] (mSv)	Percentage Error (%)
28/D4	0.71 ± 0.07	0.58 ± 0.057	22.4
27/C3	0.74 ± 0.07	0.62 ± 0.061	19.4
26/C3	0.8 ± 0.08	0.66 ± 0.059	21.2
Average	**0.75 ± 0.11[2]**	**0.62 ± 0.0.06[2]**	**21.0**

4) Results are rounded up to the nearest tenth and slice/position error is calculated as ±10% error based on phone communications with Michael Klueber at the US Air Force Radiation Dosimetry Branch.
5) Overall system error is calculated as the square root of the sum of the squares of the standard deviation and measurement error, per guidance in NCRP Report 58.
6) Error in these calculated results are expressed as relative error, where MCNP defines relative error, $R = \sigma / \bar{x}$, where σ is the standard deviation of the mean and $\bar{x}$ is the mean.

Table C8: The measured and calculated absorbed dose results for the right lung.

Slice/Position	Measured Results[1] (mSv)	Calculated Results[3] (mSv)	Percentage Error (%)
23/C1	1.25 ± 0.125	1.05 ± 0.043	19.0
23/C2	0.92 ± 0.092	0.75 ± 0.040	22.7
23/C3	0.77 ± 0.077	0.63 ± 0.039	22.2
23/C4	0.66 ± 0.066	0.51 ± 0.048	29.4
23/D1	1.18 ± 0.118	0.99 ± 0.041	19.2
23/D2	0.99 ± 0.099	0.85 ± 0.042	16.5
23/D3	0.8 ± 0.08	0.65 ± 0.048	23.1
23/D4	0.68 ± 0.068	0.55 ± 0.043	23.6
22/C1	1.2 ± 0.12	1.01 ± 0.042	18.8
22/C2	0.92 ± 0.092	0.74 ± 0.018	24.3
22/C3	0.76 ± 0.076	0.65 ± 0.042	16.9
22/C4	0.68 ± 0.068	0.56 ± 0.045	21.4
22/D1	1.16 ± 0.116	0.95 ± 0.044	22.1
22/D2	0.91 ± 0.091	0.73 ± 0.046	24.7
22/D3	0.77 ± 0.077	0.64 ± 0.060	20.3
22/D4	0.66 ± 0.066	0.51 ± 0.054	29.4
21/C1	1.06 ± 0.106	0.89 ± 0.042	19.1
21/C2	0.92 ± 0.092	0.75 ± 0.054	22.7
21/C3	0.82 ± 0.082	0.67 ± 0.044	22.4
21/C4	0.64 ± 0.064	0.56 ± 0.021	14.3
21/D1	1.05 ± 0.105	0.87 ± 0.041	20.7
21/D2	0.93 ± 0.093	0.77 ± 0.041	20.8
21/D3	0.78 ± 0.078	0.66 ± 0.041	18.2
21/D4	0.65 ± 0.065	0.52 ± 0.044	25.0
20/C2	0.94 ± 0.094	0.79 ± 0.043	19.0
20/C3	0.75 ± 0.075	0.64 ± 0.058	17.2
20/C4	0.62 ± 0.062	0.51 ± 0.043	21.6
20/D1	1.04 ± 0.104	0.86 ± 0.041	20.9
20/D2	0.9 ± 0.09	0.75 ± 0.042	20.0
20/D3	0.72 ± 0.072	0.59 ± 0.051	22.0
20/D4	0.62 ± 0.062	0.52 ± 0.044	19.2
20/E3	0.77 ± 0.077	0.64 ± 0.061	20.3
19/C2	0.84 ± 0.084	0.71 ± 0.043	18.3
19/C3	0.77 ± 0.077	0.63 ± 0.044	22.2
19/C4	0.69 ± 0.069	0.58 ± 0.043	19.0
19/D1	1 ± 0.1	0.81 ± 0.040	23.5

19/D2	0.92 ± 0.092	0.75 ± 0.041	22.7
19/D3	0.79 ± 0.079	0.68 ± 0.047	16.2
19/D4	0.67 ± 0.067	0.59 ± 0.038	13.6
19/E3	0.72 ± 0.072	0.58 ± 0.045	24.1
18/C2	0.94 ± 0.094	0.77 ± 0.044	22.1
18/C3	0.77 ± 0.077	0.61 ± 0.043	26.2
18/D1	0.97 ± 0.097	0.81 ± 0.043	19.8
18/D2	0.9 ± 0.09	0.77 ± 0.045	16.9
18/D3	0.79 ± 0.079	0.67 ± 0.050	17.9
18/D4	0.7 ± 0.07	0.55 ± 0.044	27.3
18/E2	0.97 ± 0.097	0.85 ± 0.056	14.1
18/E3	0.85 ± 0.085	0.74 ± 0.018	14.9
17/C2	0.86 ± 0.086	0.68 ± 0.022	26.5
17/C3	0.81 ± 0.081	0.66 ± 0.038	22.7
17/D1	0.93 ± 0.093	0.79 ± 0.046	17.7
17/D2	0.88 ± 0.088	0.74 ± 0.044	18.9
17/D3	0.82 ± 0.082	0.71 ± 0.041	15.5
17/D4	0.73 ± 0.073	0.61 ± 0.039	19.7
17/E2	0.88 ± 0.088	0.76 ± 0.043	15.8
17/E3	0.86 ± 0.086	0.75 ± 0.043	14.7
16/C2	0.8 ± 0.08	0.65 ± 0.076	23.1
16/C3	0.73 ± 0.073	0.58 ± 0.071	25.9
16/D1	0.93 ± 0.093	0.79 ± 0.049	17.7
16/D2	0.83 ± 0.083	0.71 ± 0.047	16.9
16/D3	0.82 ± 0.082	0.68 ± 0.048	20.6
16/D4	0.78 ± 0.078	0.65 ± 0.043	20.0
16/E2	0.83 ± 0.083	0.7 ± 0.046	18.6
16/E3	0.8 ± 0.08	0.69 ± 0.038	15.9
Average	**0.85 ± 0.17[2]**	**0.70 ± 0.04[2]**	**20.4**

1) Results are rounded up to the nearest tenth and slice/position error is calculated as ±10% error based on phone communications with Michael Klueber at the US Air Force Radiation Dosimetry Branch.
2) Overall system error is calculated as the square root of the sum of the squares of the standard deviation and measurement error, per guidance in NCRP Report 58.
3) Error in these calculated results are expressed as relative error, where MCNP defines relative error, $R = \sigma / \bar{x}$, where σ is the standard deviation of the mean and $\bar{x}$ is the mean.

C.2 Monitoring Period Two Organ Specific Results

Table C9: The measured and calculated absorbed dose results for the small intestine.

Slice/Position	Measured Results[1] (mSv)	Calculated Results[3] (mSv)	Percentage Error (%)
31/A1	1.23 ± 0.12	1.15 ± 0.045	7.0
31/C1	1.11 ± 0.11	1.08 ± 0.045	2.8
31/E3	0.91 ± 0.09	0.62 ± 0.085	46.8
31/F3	0.9 ± 0.09	0.74 ± 0.065	21.6
31/F5	0.8 ± 0.08	0.59 ± 0.085	35.6
30/A1	1.28 ± 0.13	1.02 ± 0.049	25.5
30/C1	1.08 ± 0.11	0.98 ± 0.055	10.2
30/E3	0.92 ± 0.09	0.65 ± 0.050	41.5
Average	**1.03 ± 0.19[2]**	**0.85 ± 0.06[2]**	**23.9**

1) Results are rounded up to the nearest tenth and slice/position error is calculated as ±10% error based on phone communications with Michael Klueber at the US Air Force Radiation Dosimetry Branch.
2) Overall system error is calculated as the square root of the sum of the squares of the standard deviation and measurement error, per guidance in NCRP Report 58.
3) Error in these calculated results are expressed as relative error, where MCNP defines relative error, $R = \sigma / \bar{x}$, where σ is the standard deviation of the mean and $\bar{x}$ is the mean,

Table C10: The measured and calculated absorbed dose results for the kidney.

Slice/Position	Measured Results[1] (mSv)	Calculated Results[3] (mSv)	Percentage Error (%)
31/A3	0.9 ± 0.09	0.65 ± 0.05	38.5
31/C3	0.78 ± 0.078	0.65 ± 0.06	20.0
30/A3	0.76 ± 0.076	0.63 ± 0.06	20.6
30/C3	0.77 ± 0.077	0.61 ± 0.049	26.2
29/A3	0.86 ± 0.086	0.72 ± 0.0365	19.4
28/A3	0.87 ± 0.087	0.68 ± 0.05	27.9
28/B3	0.79 ± 0.079	0.65 ± 0.055	21.5
27/A3	0.83 ± 0.083	0.73 ± 0.0375	13.7
27/B3	0.79 ± 0.079	0.69 ± 0.065	14.5
Average	**0.82 ± 0.11[2]**	**0.67 ± 0.05[2]**	**22.5**

1) Results are rounded up to the nearest tenth and slice/position error is calculated as ±10% error based on phone communications with Michael Klueber at the US Air Force Radiation Dosimetry Branch.
2) Overall system error is calculated as the square root of the sum of the squares of the standard deviation and measurement error, per guidance in NCRP Report 58.
3) Error in these calculated results are expressed as relative error, where MCNP defines relative error, $R = \sigma / \bar{x}$, where σ is the standard deviation of the mean and $\bar{x}$ is the mean.

Table C11: The measured and calculated absorbed dose results for the liver.

Slice/Position	Measured Results[1] (mSv)	Calculated Results[3] (mSv)	Percentage Error (%)
29/A1	1.34 ± 0.13	0.91 ± 0.050	47.3
29/C1	1.14 ± 0.11	0.91 ± 0.049	25.3
29/C3	0.83 ± 0.08	0.55 ± 0.051	50.9
29/E1	1.16 ± 0.12	1.08 ± 0.050	7.4
28/A1	1.21 ± 0.12	1.1 ± 0.054	10.0
28/B1	1.27 ± 0.13	1.02 ± 0.048	24.5
28/C1	1.15 ± 0.12	0.99 ± 0.054	16.2
28/C3	0.77 ± 0.08	0.59 ± 0.063	30.5
27/B1	1.24 ± 0.12	0.87 ± 0.049	42.5
27/C1	1.15 ± 0.12	0.89 ± 0.049	29.2
27/D4	0.71 ± 0.07	0.53 ± 0.088	34.0
26/B1	1.36 ± 0.14	1.1 ± 0.051	23.6
26/C1	1.2 ± 0.12	1.04 ± 0.046	15.4
26/D4	0.69 ± 0.07	0.58 ± 0.090	19.0
25/C1	1.32 ± 0.13	1.16 ± 0.050	13.8
25/C2	0.98 ± 0.10	0.74 ± 0.062	32.4
25/C3	0.8 ± 0.08	0.68 ± 0.058	17.6
25/C4	0.68 ± 0.07	0.54 ± 0.080	25.9
25/D1	1.3 ± 0.13	1.15 ± 0.058	13.0
25/D2	0.96 ± 0.10	0.75 ± 0.061	28.0
25/D3	0.85 ± 0.09	0.62 ± 0.065	37.1
25/D4	0.66 ± 0.07	0.61 ± 0.089	8.2
24/C1	1.29 ± 0.13	1.08 ± 0.050	19.4
24/C2	1.04 ± 0.10	0.81 ± 0.064	28.4
24/C3	0.81 ± 0.08	0.61 ± 0.064	32.8
24/C4	0.66 ± 0.07	0.51 ± 0.073	29.4
24/D1	1.23 ± 0.12	1 ± 0.047	23.0
24/D2	1 ± 0.10	0.82 ± 0.051	22.0
24/D3	0.83 ± 0.08	0.68 ± 0.060	22.1
24/D4	0.69 ± 0.07	0.54 ± 0.093	27.8
Average	**1.01 ± 0.26[2]**	**0.82 ± 0.06[2]**	**25.2**

1) Results are rounded up to the nearest tenth and slice/position error is calculated as ±10% error based on phone communications with Michael Klueber at the US Air Force Radiation Dosimetry Branch.
2) Overall system error is calculated as the square root of the sum of the squares of the standard deviation and measurement error, per guidance in NCRP Report 58.
3) Error in these calculated results are expressed as relative error, where MCNP defines relative error, $R = \sigma / \bar{x}$, where σ is the standard deviation of the mean and $\bar{x}$ is the mean.

Table C12: The measured and calculated absorbed dose results for the ascending colon.

Slice/Position	Measured Results[1] (mSv)	Calculated Results[3] (mSv)	Percentage Error (%)
31/E1	1.28 ± 0.13	0.97 ± 0.057	32.0
30/E1	1.26 ± 0.13	0.95 ± 0.050	32.6
29/E3	0.85 ± 0.09	0.67 ± 0.088	26.9
Average	**1.13 ± 0.22[2]**	**0.86 ± 0.07[2]**	**30.5**

1) Results are rounded up to the nearest tenth and slice/position error is calculated as ±10% error based on phone communications with Michael Klueber at the US Air Force Radiation Dosimetry Branch.
2) Overall system error is calculated as the square root of the sum of the squares of the standard deviation and measurement error, per guidance in NCRP Report 58.
3) Error in these calculated results are expressed as relative error, where MCNP defines relative error, $R = \sigma / \bar{x}$, where σ is the standard deviation of the mean and $\bar{x}$ is the mean.

Table C13: The measured and calculated absorbed dose results for the transverse colon.

Slice/Position	Measured Results[1] (mSv)	Calculated Results[3] (mSv)	Percentage Error (%)
30/F3	1.02 ± 0.10	0.75 ± 0.048	36.0
30/F5	0.72 ± 0.07	0.61 ± 0.041	18.0
29/F3	1.01 ± 0.10	0.74 ± 0.047	36.5
29/F5	0.72 ± 0.07	0.62 ± 0.042	16.1
Average	**0.87 ± 0.18[2]**	**0.68 ± 0.04[2]**	**26.7**

1) Results are rounded up to the nearest tenth and slice/position error is calculated as ±10% error based on phone communications with Michael Klueber at the US Air Force Radiation Dosimetry Branch.
2) Overall system error is calculated as the square root of the sum of the squares of the standard deviation and measurement error, per guidance in NCRP Report 58.
3) Error in these calculated results are expressed as relative error, where MCNP defines relative error, $R = \sigma / \bar{x}$, where σ is the standard deviation of the mean and $\bar{x}$ is the mean.

Table C14: The measured and calculated absorbed dose results for the gall bladder.

Slice/Position	Measured Results[1] (mSv)	Calculated Results[3] (mSv)	Percentage Error (%)
28/D2	1.03 ± 0.102	0.75 ± 0.005	27.2
27/D2	1.02 ± 0.072	0.68 ± 0.056	25.9
26/D2	0.97 ± 0.101	0.76 ± 0.005	26.0
Average	**1.01 ± 0.10[2]**	**0.73 ± 0.03[2]**	**26.4**

1) Results are rounded up to the nearest tenth and slice/position error is calculated as ±10% error based on phone communications with Michael Klueber at the US Air Force Radiation Dosimetry Branch.
2) Overall system error is calculated as the square root of the sum of the squares of the standard deviation and measurement error, per guidance in NCRP Report 58.
3) Error in these calculated results are expressed as relative error, where MCNP defines relative error, $R = \sigma / \bar{x}$, where σ is the standard deviation of the mean and $\bar{x}$ is the mean.

Table C15: The measured and calculated absorbed dose results for the pancreas.

Slice/Position	Measured Results[1] (mSv)	Calculated Results[3] (mSv)	Percentage Error (%)
28/D4	0.68 ± 0.07	0.58 ± 0.057	17.2
27/C3	0.80 ± 0.08	0.62 ± 0.061	29.0
26/C3	0.81 ± 0.08	0.66 ± 0.059	22.7
Average	**0.76 ± 0.12[2]**	**0.62 ± 0.06[2]**	**23.0**

1) Results are rounded up to the nearest tenth and slice/position error is calculated as ±10% error based on phone communications with Michael Klueber at the US Air Force Radiation Dosimetry Branch.
2) Overall system error is calculated as the square root of the sum of the squares of the standard deviation and measurement error, per guidance in NCRP Report 58.
3) Error in these calculated results are expressed as relative error, where MCNP defines relative error, $R = \sigma / \bar{x}$, where σ is the standard deviation of the mean and $\bar{x}$ is the mean.

Table C16: The measured and calculated absorbed dose results for the right lung.

Slice/Position	Measured Results[1] (mSv)	Calculated Results[3] (mSv)	Percentage Error (%)
23/C1	1.26 ± 0.13	1.05 ± 0.043	20.0
23/C2	1.00 ± 0.10	0.75 ± 0.040	33.3
23/C3	0.79 ± 0.08	0.63 ± 0.039	25.4
23/C4	0.68 ± 0.07	0.51 ± 0.048	33.3
23/D1	1.26 ± 0.13	0.99 ± 0.041	27.3
23/D2	1.01 ± 0.10	0.85 ± 0.042	18.8
23/D3	0.83 ± 0.08	0.65 ± 0.048	27.7
23/D4	0.73 ± 0.07	0.55 ± 0.043	32.7
22/C1	1.2 ± 0.12	1.01 ± 0.042	18.8
22/C2	0.98 ± 0.10	0.74 ± 0.018	32.4
22/C3	0.75 ± 0.08	0.65 ± 0.042	15.4
22/C4	0.68 ± 0.07	0.56 ± 0.045	21.4
22/D1	1.14 ± 0.11	0.95 ± 0.044	20.0
22/D2	0.97 ± 0.10	0.73 ± 0.046	32.9
22/D3	0.78 ± 0.08	0.64 ± 0.060	21.9
22/D4	0.72 ± 0.07	0.51 ± 0.054	41.2
21/C1	1.1 ± 0.11	0.89 ± 0.042	23.6
21/C2	0.95 ± 0.10	0.75 ± 0.054	26.7
21/C3	0.75 ± 0.08	0.67 ± 0.044	11.9
21/C4	0.68 ± 0.07	0.56 ± 0.021	21.4
21/D1	1.1 ± 0.11	0.87 ± 0.041	26.4
21/D2	0.91 ± 0.09	0.77 ± 0.041	18.2
21/D3	0.83 ± 0.08	0.66 ± 0.041	25.8
21/D4	0.65 ± 0.07	0.52 ± 0.044	25.0
20/C2	1.0 ± 0.10	0.79 ± 0.043	26.6
20/C3	0.8 ± 0.08	0.64 ± 0.058	25.0
20/C4	0.63 ± 0.06	0.51 ± 0.043	23.5
20/D1	1.15 ± 0.12	0.86 ± 0.041	33.7
20/D2	0.93 ± 0.09	0.75 ± 0.042	24.0
20/D3	0.8 ± 0.08	0.59 ± 0.051	35.6
20/D4	0.67 ± 0.07	0.52 ± 0.044	28.8
20/E3	0.8 ± 0.08	0.64 ± 0.061	25.0
19/C2	0.93 ± 0.09	0.71 ± 0.043	31.0
19/C3	0.82 ± 0.08	0.63 ± 0.044	30.2
19/C4	0.69 ± 0.07	0.58 ± 0.043	19.0
19/D1	1.02 ± 0.10	0.81 ± 0.040	25.9

19/D2	0.97 ± 0.10	0.75 ± 0.041	29.3
19/D3	0.76 ± 0.08	0.68 ± 0.047	11.8
19/D4	0.63 ± 0.06	0.59 ± 0.038	6.8
19/E3	0.72 ± 0.07	0.58 ± 0.045	24.1
18/C2	0.94 ± 0.09	0.77 ± 0.044	22.1
18/C3	0.8 ± 0.08	0.61 ± 0.043	31.1
18/D1	0.98 ± 0.10	0.81 ± 0.043	21.0
18/D2	0.95 ± 0.10	0.77 ± 0.045	23.4
18/D3	0.84 ± 0.08	0.67 ± 0.050	25.4
18/D4	0.7 ± 0.07	0.55 ± 0.044	27.3
18/E2	0.97 ± 0.10	0.85 ± 0.056	14.1
18/E3	0.84 ± 0.08	0.74 ± 0.018	13.5
17/C2	0.99 ± 0.10	0.68 ± 0.022	45.6
17/C3	0.85 ± 0.09	0.66 ± 0.038	28.8
17/D1	1.0 ± 0.10	0.79 ± 0.046	26.6
17/D2	0.98 ± 0.10	0.74 ± 0.044	32.4
17/D3	0.86 ± 0.09	0.71 ± 0.041	21.1
17/D4	0.76 ± 0.08	0.61 ± 0.039	24.6
17/E2	0.97 ± 0.10	0.76 ± 0.043	27.6
17/E3	0.85 ± 0.09	0.75 ± 0.043	13.3
16/C2	0.84 ± 0.08	0.65 ± 0.076	29.2
16/C3	0.83 ± 0.08	0.58 ± 0.071	43.1
16/D1	1.04 ± 0.10	0.79 ± 0.049	31.6
16/D2	0.9 ± 0.09	0.71 ± 0.047	26.8
16/D3	0.86 ± 0.09	0.68 ± 0.048	26.5
16/D4	0.79 ± 0.08	0.65 ± 0.043	21.5
16/E2	0.91 ± 0.09	0.7 ± 0.046	30.0
16/E3	0.96 ± 0.10	0.69 ± 0.038	39.1
Average	**0.88 ± 0.18[2]**	**0.70 ± 0.09[2]**	**25.7**

1) Results are rounded up to the nearest tenth and slice/position error is calculated as ±10% error based on phone communications with Michael Klueber at the US Air Force Radiation Dosimetry Branch.
2) Overall system error is calculated as the square root of the sum of the squares of the standard deviation and measurement error, per guidance in NCRP Report 58.
3) Error in these calculated results are expressed as relative error, where MCNP defines relative error, $R = \sigma / \bar{x}$, where σ is the standard deviation of the mean and $\bar{x}$ is the mean.

VITA

David Wayne Hearnsberger received his Bachelor of Science in radiological health engineering and Master of Science in health physics from Texas A&M University in 2001, and his Doctor of Philosophy in nuclear engineering degree from Texas A&M University in 2006. His research interests include applied health physics and radiation dosimetry. He can be reached at 8005 Outer Circle Road, Brooks City-Base, Texas 78235.

Publications

Office of Civilian Radioactive Waste Management (OCRWM), Characterization Survey of the Yucca Mountain Land Withdraw. Las Vegas, NV: Office of Civilian Radioactive Waste Management; February 2005.

Hearnsberger, D.W. Fission Neutron/Gamma Irradiation of Bacillus thuringiensis at the Texas A&M University Nuclear Science Center Reactor. Texas A&M University: Thesis Office; August 2001.

Hearnsberger, D.W. 1998 Assessment of Dissolved Radon-222 in Drinking Water at the Bryan/College Station, Texas Watershed. Health Physics Journal, 74(6), 720 June 1998.

Presentations

Hearnsberger, D.W. Emergency Responses Involving a Radiological Dispersal Device or an Improvised Nuclear Device, Presented to Tetra Tech EM, Inc; March 2006.

Hearnsberger, D.W. Coworker Dosimetry Distributions Used in Dose Reconstruction, Presented to the Health Physics Society; July 2005.

Hearnsberger, D.W. The MARSSIM Process, An Overview, Presented to the Department of Energy, Office of Repository Development; October 2004.

Hearnsberger, D.W. Technical Basis Document User's Guide Development for Radiation Dose Reconstruction. Cincinnati, OH: Office of Compensation Analysis and Support: September 2004.

Hearnsberger, D.W. Decommissioning the High Pressure Tritium Facility at the Los Alamos National Laboratory. Presented to the Waste Management Conference; February 2003.

Hearnsberger, D.W. Bioterrorism or Natural Outbreak: A Clinical or Diagnostic Pathological Approach? Presented to Texas A&M University, Department of Medical Microbiology; October 2002.